Emergent Materials
https://doi.org/10.1007/s42247-021-00226-1

REVIEW

Collagen biomineralization: pathways, mechanisms, and thermodynamics

Lioudmila V. Sorokina[1] · Reza Shahbazian-Yassar[1,2] · Tolou Shokuhfar[2,3]

Received: 5 September 2020 / Accepted: 16 April 2021

Abstract

Over the past two decades, numerous studies have investigated and characterized the transient and amorphous phases in early stages of mineralization as well as their transition mechanisms to apatite crystals in buffered solutions. Recently more attention has been drawn to the identification and characterization of collagen structure and how it can affect mineralization in contact with non-collagenous protein and calcium phosphate clusters. This review highlights some of the pathways and mechanisms through which amorphous calcium phosphate clusters form. The conversion of these clusters into hydroxyapatite crystals is also reviewed. The thermodynamic aspects of nucleation and growth processes based on classical and non-classical nucleation theories related to hydroxyapatite are discussed. In addition, this paper is written to address the significant progress on mechanisms and pathways engaged in mineralization of collagen fibrils. Finally, it addresses some of the breakthroughs and limitations in the field of collagen biomineralization studies and new challenges in this field of study.

Keywords Collagen biomineralization · Collagen fibrils · Nucleation and growth process · Calcium phosphate

1 Introduction

Biomineralization is an intricate process by which living organisms produce minerals such as carbonates and phosphates. Tissue matrices, and the area around them, provide compartments for these minerals to deposit [1]. The mineralization onto collagen, a protein that is present in many organisms, is a scenario in which water within its matrix is completely replaced with calcium and phosphate precipitants [2]. This phenomenon provides mechanical support for many types of organisms from unicellular organisms to large mammalian ones. However, in vivo exploration of collagen biomineralization is complicated due to the numerous mechanisms that are occurring simultaneously within any tissue. Therefore, in vitro models are sometime used to simplify mechanism of biomineralization, for this paper, the precipitate within collagen fibrils [3].

An important precipitate in collagen fibrils is hydroxyapatite (HA). While the formation of HA can require multiple steps, the first stage usually requires the presence of both calcium and phosphate ions, often supersaturated in solution. These ions then aggregate to form amorphous nanoclusters or calcium phosphate complexes [1]. Calcium phosphate complexes are among the more well-studied biomineralization complexes. In addition they are known as precursors of HA which is the predominant inorganic component in mammalian hard tissue such as bone, teeth of vertebrates [4]. Understanding the physiological HA formation in bone is key to creating biomaterials. Figure 1 demonstrates the role of HA in the hierarchy of bone formation. The pathological calcification also cannot be understated as biomineralization is present in diseases such as calcific tendonitis, gallstones, and others.

The pathways and mechanisms of HA formation in collagen fibrils can be studied by reviewing the kinetics and mechanisms associated with nucleation. Broadly, nucleation can be broken into classical and non-classical nucleation [6]. Both nucleation processes are defined in sections later in the paper. However, understanding the nucleation and growth processes of calcium phosphate minerals is vital for numerous biological and tissue engineering applications [7].

✉ Tolou Shokuhfar
tolou@uic.edu

[1] Department of Civil and Materials Engineering, University of Illinois at Chicago, Chicago, IL 60607, USA

[2] Department of Mechanical and Industrial Engineering, University of Illinois at Chicago, Chicago, IL 60607, USA

[3] Department of Bioengineering, University of Illinois at Chicago, Chicago, IL 60607, USA

Published online: 19 June 2021

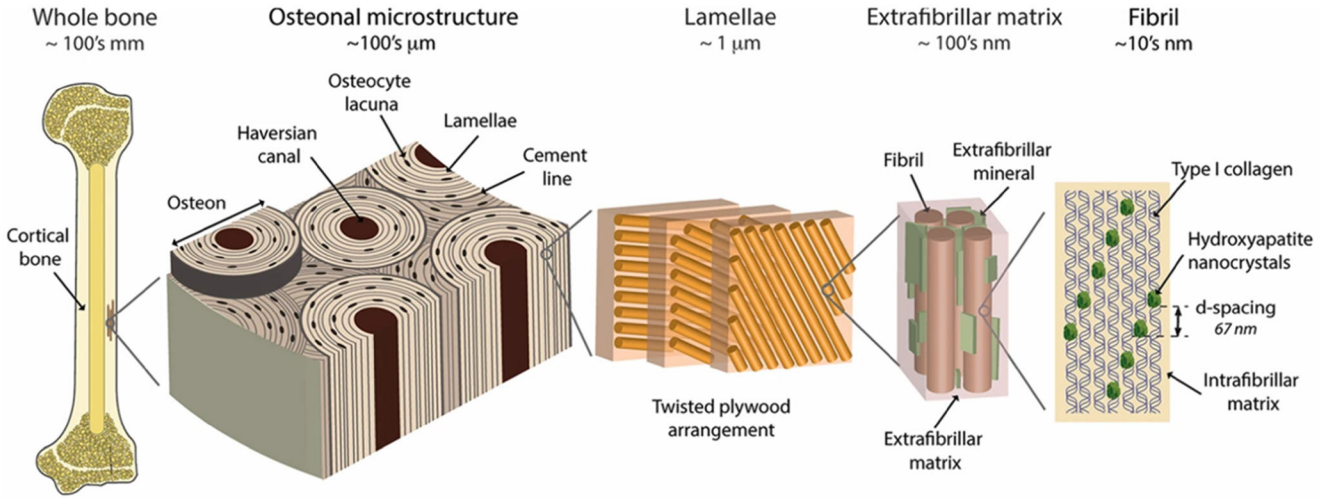

Fig. 1 Hierarchical structure of bone hydroxyapatite. On the macroscale, bone can be subdivided as compact on the exterior and spongy on the interior. The former is composed of osteons, containing a mineral matrix and osteocytes and Haversian canals surrounding the blood vessels. The lamellar structure of osteons is made up of an interwoven network of collagen fibers, which consist of collagen fibrils. The structure of a collagen fibril presents three chains of amino acids formed in a triple helix and crystals of hydroxyapatite, composed of calcium and phosphorus. Reprinted with permission from [5]

This review discusses thermodynamic and kinetic aspects of biological nucleation and growth processes. In addition, mechanisms and pathways of biomineralization within collagen matrix are discussed. Finally, elementary features of formation and transformation of amorphous calcium phosphate (ACP) into more stable phase are addressed.

2 Classic nucleation theory

Classical nucleation theory (CNT) emerged with Gibbs's work in the late nineteenth century [5, 8]. CNT enables us to understand the nucleation of a thermodynamic phase in a solution. It also provides some reasonable assumptions to estimate nucleation rate [9]. According to CNT, nucleation begins through the attachment of monomers on the surface of growing particle, as schematically shown in Fig. 2a. In a supersaturated solution, a balance between the surface and bulk Gibbs free energy, ΔG_S and theΔG_b, respectively, determines the withering or growth of the nanoparticle. If the particle is assumed to be a sphere, the surface energy scales with square of its radius (r) and bulk energy scales with cube of its radius (r). Figure 2b schematically shows what happens to the ΔG as the nanosized particle grows, while Eq. 1 details out the mathematical formula [10].

$$\Delta G = \Delta G_b + \Delta G_s \rightarrow \Delta G = -\left\{\frac{\left[\left(\frac{4}{3}\right)\pi r^3\right]}{V_m}\right\} k_B T\sigma + 4\pi r^2 \alpha \qquad (1)$$

In Eq. 1, α represents the interfacial energy, k_B is the Boltzmann's constant, T represents the temperature in Kelvin, σ is the supersaturation value, and V_m is the volume per molecule of nucleus.

It is possible to derive the critical radius needed, r_c, for the nucleation to grow and its ΔG_n. Both are shown below in Eqs. 2 and 3, respectively

$$r_c = \frac{2\alpha V_m}{k_B T\sigma} \qquad (2)$$

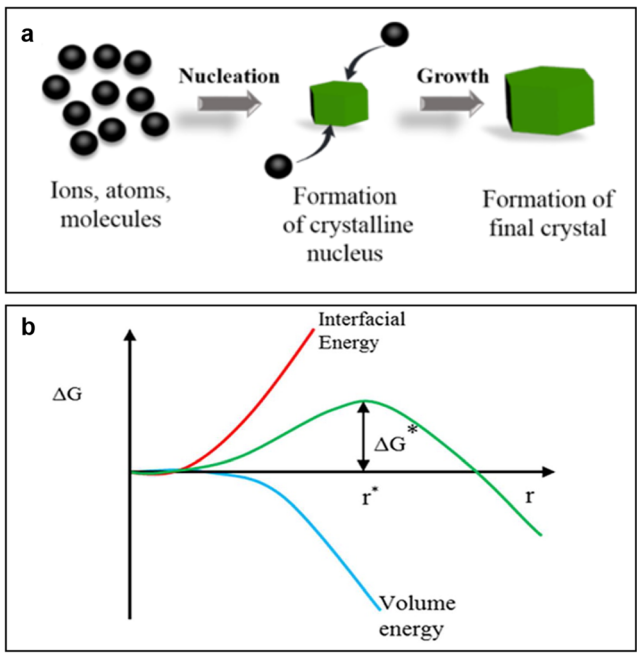

Fig. 2 **a** Classical nucleation begins through particle attachment on the surface of a growing particle based on CNT. **b** Schematic of how the Gibbs free energy is a function of the size of the nucleus and how everything relates to the combination of surface (interfacial) and bulk energy. Reprinted with permission from [9]

$$\Delta G_n = \frac{16\pi V_m \alpha^3}{3k_B{}^2 T^2 \sigma^2} \quad (3)$$

In the classical perspective of crystallization, growth process proceeds via formation of many stable particles. However, it does not take into consideration the ability of several small nuclei, with radius below the critical radius, encountering each other and potentially leading to growth of nucleus.

3 Non-classical nucleation theory

Recent observations have shown that nucleation process of a crystal can occur when nuclei come into contact with each other forming a larger particle [11]. This is referred to as non-classic nucleation. This behavior, known as the Oswald's step rule, occurs in complex materials such as polymeric solutions, minerals, and colloids. Oswald's rule expresses that an unstable phase does not transform directly to a more stable phase. It tends to reach an intermediate phase which is close to initial phase in term of total free energy. The existence of these intermediate phases can effectively minimize energy barrier of nucleation. This is because these intermediate equilibrium points affect both the values of α and σ, causing a smaller ΔG_n. This in turn increases the likelihood of each intermediate step to occur. As a result, intermediate steps can occur at supersaturation levels lower than those in CNT [11]. Thus, nucleation proceeds via non-classical nucleation theory (also known as two-step nucleation process). First step is the formation of clusters in the solution having critical radius. Second step initiates through the formation of crystalline nucleus via rearranging the lattice structure of cluster. The non-classical nucleation will occur when the energy required is less than that of CNT [9]. This is shown in Fig. 3b–c. Figure 3 also shows the total free energy difference in two classical and non-classical theories in the presence of an intermediate phase. However, the total free energy-related equations obtained for CNT can also be considered for non-classical pathway. In Eq. 1 the sign of the ΔG_s is positive leading it to act as a nucleation energy barrier, especially when $r \ll r_c$. From the same equation, increasing particle size beyond r_c leads to stability of the particles. Consequently, total free energy or nucleation energy barrier is controlled by bulk free energy term.

From the mineralization perspective, pre-nucleation clusters (PNCs) in solution play a vital role in early steps of nucleation process [15]. What differentiates PNCs from other nuclei is unlike CNT nuclei which are solid, and PNCs are clusters of molecules often in aqueous form and thus are amorphous liquid clusters. PNCs could aggregate to form an intermediate, transient and amorphous phase and mediate crystallization. This amorphous phase is known as main precursor of formation of more stable crystals [11]. Using a colloidal model, Zhang et al. investigated crystallization starting from amorphous phase [13]. Zhang et al. pointed out that amorphous clusters form in the suspension to minimize the interfacial energy, subsequently, and reduce energy barrier of nucleation. In fact, the amorphous cluster needs to reach a critical size to become metastable and to grow outwardly. Finally, due to the fact that energy barrier is lowered, crystalline nucleus begins forming from amorphous phase, as seen in Fig. 3 c, d, e, and f. Habraken et al. combined high-resolution cryogenic transmission electron microscopy and performed chemical analysis to explore non-classical pathway of hydroxyapatite crystals formation [14]. The analysis revealed that calcium triphosphate complexes (PNC) which aggregate and consume extra calcium ions from solution form amorphous calcium phosphate (ACP). Afterward, metastable phase octacalcium phosphate forms at the expense of ACP which is followed by the formation of hydroxyapatite.

4 Transformation of amorphous calcium phosphate to hydroxyapatite crystals

4.1 Dissolution-precipitation mechanism

Dissolution-precipitation mechanism was firstly proposed by Blumenthal et al. who stated that there are three fundamental steps for the transformation of HA from ACP, as shown in Fig. 4a, follows a non-classical method of nucleation colloidal growth [16]. The first step is the dissolution and hydrolysis of calcium and phosphate ions initiates on the surface of ACP. The second step is the movement of hydrated ions through the surface of ACP. The third and final step is that these ions nucleate and grow on the preferred side of ACP surface. These steps are well-exhibited in a study by He et al. shown in Fig. 4b–c [17] They utilized in situ liquid cell TEM to image ACP to HA transformation in real time. They demonstrated that these ions nucleate and grow on the ACP surfaces as ACP is being dissolved. In fact, growth of HA onto the surface of ACP takes place via aggregation and coalescence mechanism. Based on the Oswald step rule as a thermodynamic viewpoint of nucleation and growth, any forward moving reaction will reach lower surface energies. Because metastable phases have similar structure to their precursors in aqueous solution, they are more likely to increase their chances to nucleate. At the start of the nucleation growth process, the hydrogen bonds available in ACP are weak. Therefore, the dissolution of metastable ACP phase takes place at the ACP/solution interface. This where the hexagonal packing of Posner clusters can be transformed to long-range ordered structures of HA nuclei [19]. The dissolution rates of ACP can be obtained

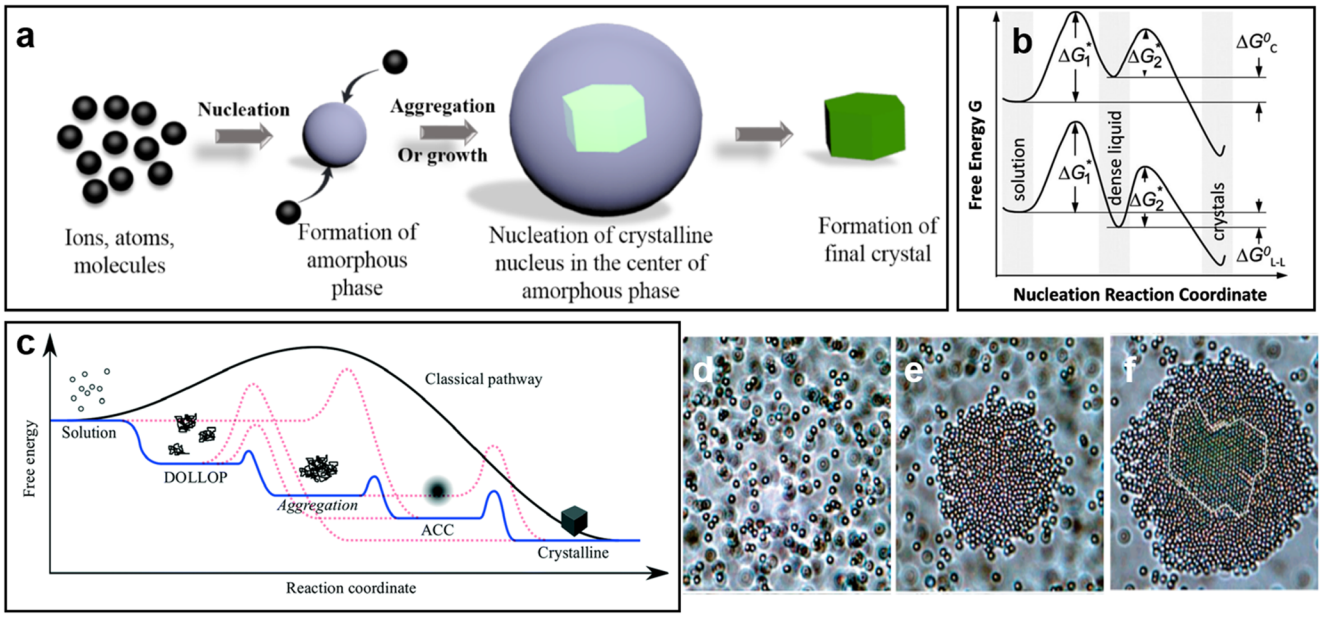

Fig. 3 **a** Nucleation proceeds via a two-step process. First step is the formation of clusters in the solution having critical radius. Second step initiates through the formation of crystalline nucleus. **b** Free energy profile of nucleation based on non-classical pathway. The graph shows changes of ΔG as a function of nucleus size$\Delta G^* = (\Delta G_2^* - \Delta G_1^*)$ stands for the large difference between energy barrier generated by small particles $r < r_c$ and large ones $r > r_c$. Reprinted with permission from [7]. **c** Variation of free energy for different crystallization pathways starting from calcium and phosphate ions. Reprinted with permission from [12]. **d** The presence of colloid molecules in the mother phase, **e** the formation of amorphous phase onto the glass surface in suspension, and **f** beginning crystallization from the core of amorphous phase. Reprinted with permission from [13]

analogous to the formation of nuclei for crystal growth based on equation below [20].

$$R(r) \approx R_\infty \left[1 - \frac{r^*}{r}\right] \tag{4}$$

Here r stands for radius of a pit, r^* is the critical radius of ACP, $R_\infty$is the velocity of dissolution at $r \to \infty$. The free energy (ΔG) is for the nucleation of a pit. Based on the CNT theory, the ΔG can be calculated by equation below.

$$\Delta G(r) = \frac{\pi r^2 h}{\Omega} kTln\sigma + 2\pi rh\alpha \tag{5}$$

In Eq. 5 r is the radius, h represents the depth of a pit, α is the interfacial free energy, Ω is molecular volume, and σ is degree of supersaturation (when $\sigma < 1$, the solution is undersaturated). And the critical size of radius (i.e., r^*) can be obtained by setting $\partial(\Delta G)/\partial(r) = 0$ leading to the equation below.

$$r^* = \frac{\alpha\Omega}{|kTln\sigma|} \tag{6}$$

Oswald step rule expresses that the least stable phase will remain in an aqueous phase. The Oswalt step rule also states that ACP to HP conversion takes place through solution-mediated mechanism. Accordingly, ACP phase dissolves and then acts as a seed to form a more stable phase, HA. These HA nanocrystals eventually aggregate to form larger crystals. Therefore, the nucleation rate is directly analogous to degree of supersaturation at the beginning of precipitation; see Eq. 7 below [21].

$$J = Aexp\left(\frac{-\beta\gamma^2 \upsilon^{4/3}}{3k^2T^2(ln\sigma)^2}\right) \tag{7}$$

In this equation, γ states the interfacial energy to form of the critical nucleus, which we can approximate to be 1.2 nm, A is pre-exponential constant, T represents the temperature in Kelvin, ν is the molecular volume-related crystallizing phase, which for HA is 5.287 × 10–28 m^3, and β is a geometric factor regarding the perimeter of the surface, in this case for cubic-like nuclei, β equals to 4.

The main driving force for the formation and aggregation mechanism of HA crystals is to minimize interfacial energy. When interfacial energy (γ) and the radius of the nucleus (r) are given, the total Gibbs free energy of the system (ΔG) is obtained by the following equation:

$$\Delta G = \frac{4}{3}\pi r^3 \Delta G_b^m + 4\,\pi r^2 \gamma \tag{8}$$

In this equation ΔG_b^m is the Gibbs free energy of the bulk HA per unit volume [22]. For the case of HA crystal in aqueous solution, γ_{SL} represents the solid-liquid interfacial energy.

For the case of aggregated HA crystal, γ_{SV} stands for the solid-gas interfacial energy. For most of the HA crystal planes, such as (100), (110) and (004) facets, the value of γ_{SL} is much larger than that of γ_{SV} [22].

ACP to HA conversion is also influenced by factors other than saturation level. These factors include pH and additives such as ions such as Mg and Si [23]. Where the driving force for HA (high supersaturation) is relatively high, pH of solution is about 10, leading to the precipitation of more stable phase of HA crystals. Based on Tung and Brown's study, a typical ACP to HA conversion kinetics experiment suggests the presence of two processes [23]. First is the consumption of acid, ACP forming into HA, when pH is less than 7 and then the reverse reaction when the pH is greater than 7. The forward reaction is shown below.

$$Ca_9(PO_4)_6 + 7H_20 \rightarrow Ca_8H_2(PO_4)_6 \cdot 5H_20 + Ca^{2+} + 2OH^-$$

To confirm previous study, Lazic showed that pH value significantly impacts the content of Posner clusters (also called loosely aggregated PNCs) [24]. The study showed that at a pH greater than 7 HA growth units form such as protonated phosphate and hydrated calcium ions.

Kim et al. revealed that the higher the calcium to phosphate ratio is, the faster ACP to HA conversion occurs [18]. In addition, crystallization of ACP into HA changes with various ratios of calcium to phosphate. ACP to HA transformation takes place faster in solution with higher Ca/P ratio. A significant amount of the initially formed ACP particle size will decrease rapidly due to forming ion-rich region in the solution. ACP to HA transformation occurs in a buffered solution with Ca/P ratio = 1.83 in which particle size of ACP reduces overtime as HA precipitants appear on their surface [18].

4.2 Internal rearrangement mechanism

West proposed that there is an internal rearrangement process during the ACP to HA transformation [25]. He showed that spherical structures of roughly 150 Å in diameter are specific characteristics of ACP in its amorphous phase. Afterward, ACP directly transforms into plate-like or needle-like HA via rearranging lattice structure without any change in its morphology. Abbona et al. revealed that HA nucleus forms homogeneously within the ACP particle by internal rearrangement process [26]. They showed that crystal structure of HA is frequently hexagonal and contains an arrangement of the phosphate tetrahedra surrounded by calcium ions. This is because HA crystal structure is highly dense in the (1010) directions. Ionic calcium polyhedral present in ACP structure must appropriately arrange in (1010) directions with the phosphate tetrahedra for this process to be associated with ion exchange. From the cluster growth model perspective ACP to HA transformation can occur through epitaxial matching states rearrangement. During this process, stacked $Ca_3(PO_4)_2$ pre-nucleation clusters and hydroxide and calcium ions move into the vacancies available among the PNCs [19]. Afterward, formed $Ca_9(PO_4)_6$ clusters could be building block units for growth of HA which are identical to the structure of Posner's clusters. One of the most efficient methods to quantitatively evaluate the phase transformation of the ACP to HA process is to use static light scattering (SLS). This method allows for that tracking of changes in molar mass, size, and internal structure of aggregates. Estimating intensity of scattered light from ACP aggregates helps to calculate the mean molar mass (M_w) and inertial radius (R_g). These parameters can be calculated based on equation below.

$$\frac{K_c}{\Delta R(q)} = \frac{1 + R_g^2 q^2/3}{M_w} + 2A_2 c \tag{9}$$

Here $\Delta R(q)$ is the solution's Rayleigh ratio, c stands for unique material constant, and A_2 represents the second virial coefficient [28].

Initially aggregates in the solution are considered ACP that eventually transform to HA nanocrystals. These aggregates are loosely packed and tend to minimize their energy by arranging their structure into HA nanocrystals. As transformation process proceeds, internal density and molar mass of the aggregates increase, whereas their radii remain intact. In high density, an immediate arrangement of ACP internal structure is preferred as it minimizes total free energy compared to random rearrangement of growth units. Furthermore, HA nanocrystals deposit through direct transition from ACP. As the number of particles attached to the aggregate increases, the loosely packed structural of ACP changes to closed packed structure of HA. The direct transformation of ACP to HA takes place by partially breaking ionic bonds between ACP molecules. The growth units both ACP and HA are Posner's clusters. This suggests that the transformation HA from ACP occurs by internal rearrangement process. Otherwise, the aggregates of ACP would have dissociated and then re-precipitate to overcome total free energy upon transition [20, 27, 29]. Kim et al. indicated that in the solutions with various calcium to phosphate ratios (1.67, 1.83, and 2.0), the extra calcium ions increase the ACP to HA conversion [27]. Generally, HA crystals tend to be calcium deficient and could compensate for lack of calcium from the solution, shown in Fig. 5a. The progress of crystallization is responsible for the increase in calcium to phosphate ratio confirming that internal rearrangement process is involved for ACP to HA conversion. Moreover Kim et al. used TEM and selected area electron diffraction (SAED) to investigate ACP to HA transition at reaction times of 3 and 5 h. At reaction time of 3 h, shown

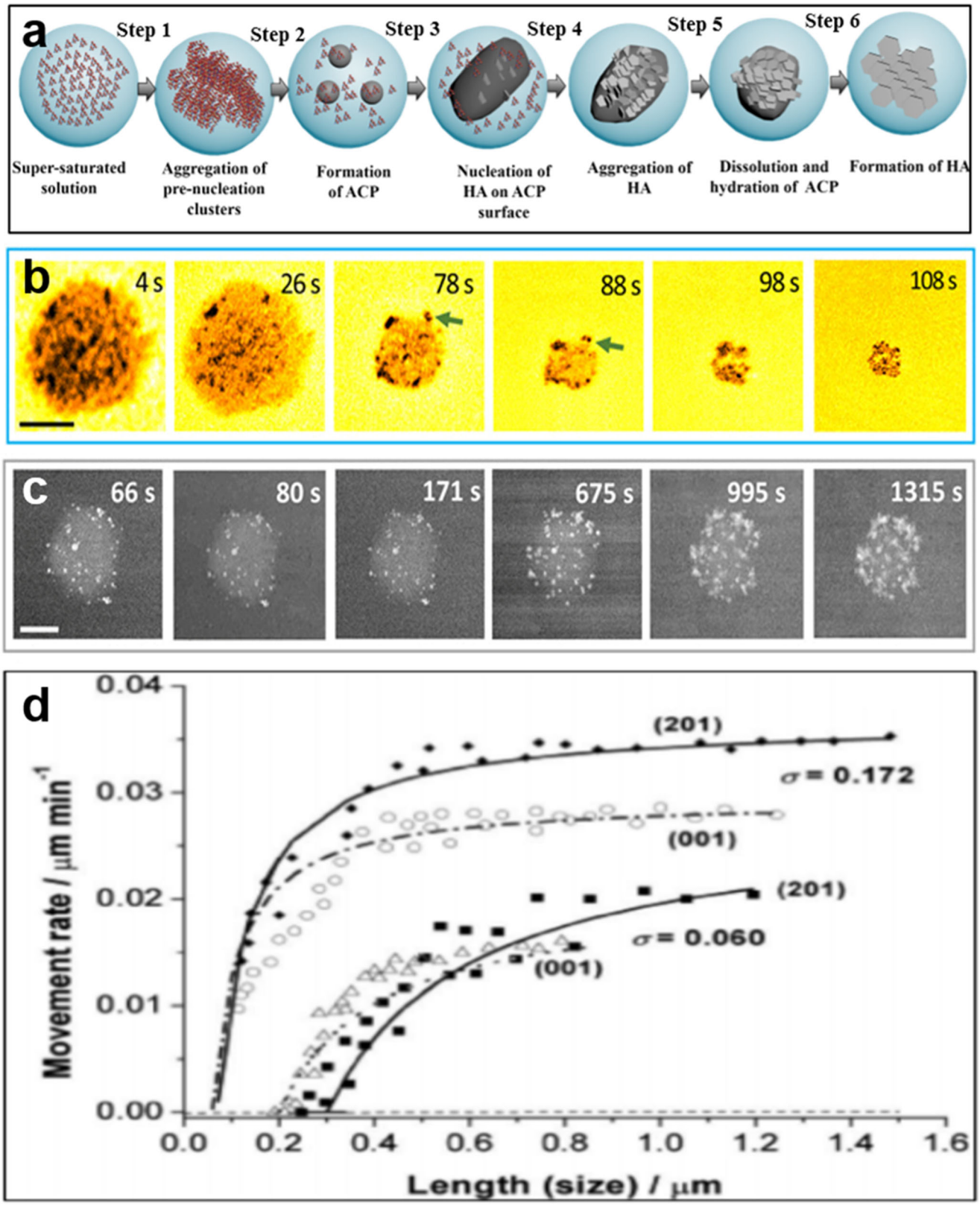

in Fig. 5b, morphology of particles is spherical, characteristic of ACP. The SAED pattern shows the presence of amorphous phase as predominant phase in the nanoparticles. However, after 5 h of reaction, a few HA nuclei are observed in dark field (DF) image as bright spots which are clearly indicated in SAED pattern.

◀ **Fig. 4** **a** Transformation of ACP to HA through dissolution-precipitation mechanism. Step 1 is the aggregation of PNCs. Step 2 is the formation of ACP. Steps 3 and 4 are the aggregation and coalescence of ACP nanoparticles and precipitation of HA nuclei on the surface of ACP. Step 5 is the dissolution and hydration of ACP. Step 6 is the conversion of ACP to HA. **b** and **c** TEM images of dissolution and precipitation of ACP particle in artificial saliva solution and heterogeneously nucleation of HA on the surface of ACP particle and growth of HA through aggregation and coalescence mechanism, respectively. Scale bars are 100 nm. Reprinted with permission from [17]. **d** Rates of pits formation as a function of size for (201) and (001) planes at under-saturation values of σ = 0.060 and 0.172, respectively. As shown, there is a direct correlation between the dissolution rate and the size (length) of the pit; under-saturation level is described by σ = 1 − S. Reprinted with permission from [19]

Somrani et al. showed that two mechanisms are engaged in amorphous tricalcium phosphate (ATCP) to HA conversion [29]. First, dissolution-precipitation mechanism occurs at high liquid-to-solid (L/S) ratios, and second, internal rearrangement phenomenon occurs at low L/S ratios. In the latter, the hydrolysis of phosphate units and the formation of hydroxide ions are vital for rearranging ATCP clusters [29, 30]. The reactions below show the beginning of internal arrangement process in ATCP clusters via hydrolysis of phosphate ions.

$$H_2O + PO_4^{-3} \rightarrow HPO_4^{-2} + OH^-$$

$$Ca_9(PO_4)_6 + H_2O \rightarrow Ca_9HPO_4PO_{45}OH$$

4.3 Kirkendall effect

Generally, atomic diffusion is possible in all states of matter, whether it is gas, liquid, or solid. Diffusion is usually far slower for solids in comparison to liquid or gas. Ernest Kirkendall was the first person who has established a mechanism for diffusion in solids [30, 31]. What was realized is that in high temperature, inter-diffusion is attributed to the movement of the interface between two different phases, so-called the Kirkendall effect. This phenomenon could take place by vacancy exchange [32]. Kirkendall effect has been studied in metal-based materials such as cobalt oxide, zinc oxide, and ferrite. However, it has not been well studied in the phase transformation of biomineralization. Tao et al. looked into this phenomenon as it relates to HA transformation from ACP [33]. Figure 6 shows how aggregation and coalescence of ACP nanoparticles occur in order to efficiently minimize the interfacial free energy. This phenomenon takes place by Ostwald ripening in which larger nanoclusters grow as smaller ones are gradually dissolved [34]. HA nanocrystals nucleate on ACP/solution interface and expand outwardly, and HA transformation begins by material flow flux from internal structure of ACP. According to Kirkendall effect, inter-diffusion of two phases at the interface depends on their diffusion flux. Any significant difference in flux for two phases might bring about to a directional flow of matter at their interface. When the diffusion flux toward shell is larger than toward the

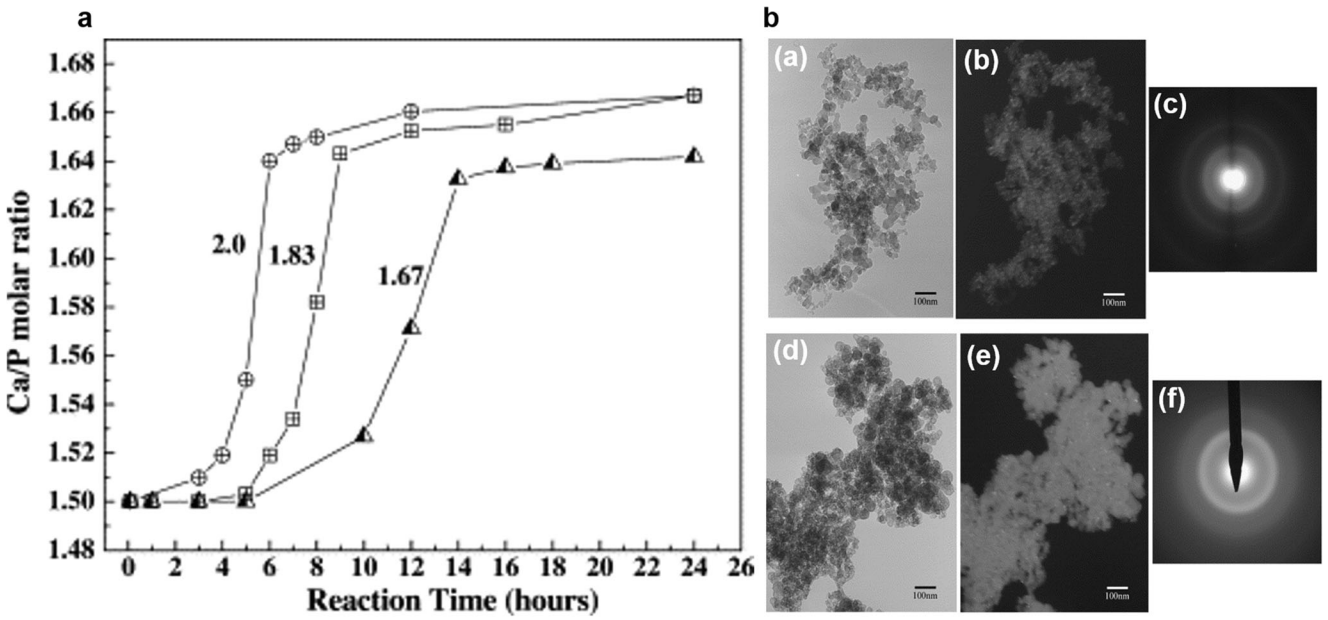

Fig. 5 **a** Impact of Ca/P ratios (1.67, 1.83, and 2) on reaction time of ACP to HA transformation. Extra Ca ions increase conversion rate of ACP to HA. Reprinted with permission from [27]. **b** TEM images of transforming ACP particles to HA via internal rearrangement process. (a), (b), and (c) show bright field (BF), dark field (DF) images, and SAED pattern of specimen at reaction time of 3 h, respectively, indicating that predominant phase is ACP, whereas (d), (e), and (f) illustrate BF, DF images and SAED pattern of specimen at reaction time of 5 h, respectively. Bright spots in DF image indicates the presence of HA nuclei onto the surfaces of ACP particles, and crystallinity is observed in SAED pattern. Reprinted with permission from [27]

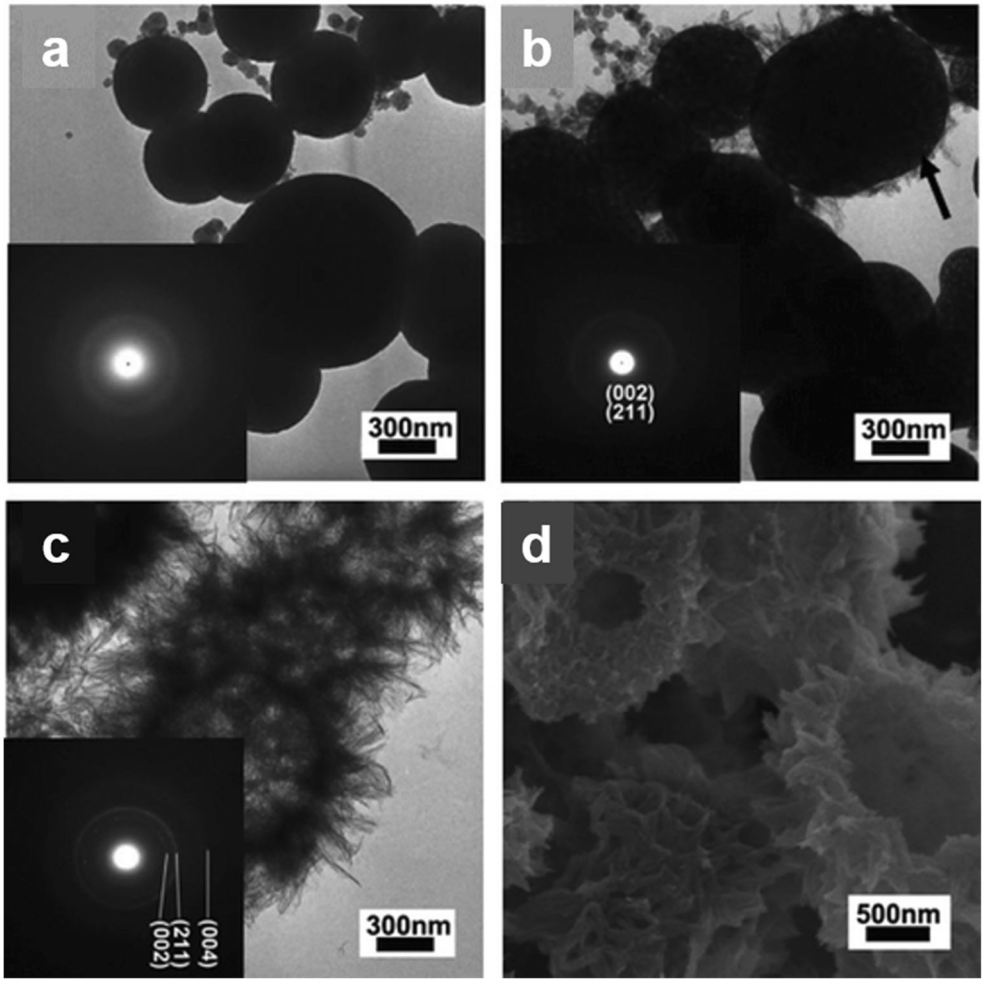

Fig. 6 TEM and SEM images of ACP-to-HA transition via Kirkendall effect coupled with surface crystallization. **a** TEM images of ACP nanoparticles, **b** aggregation of ACP nanoparticles and formation of large ACP particle, and **c** nucleation and growth of HA on the surface of HA through diffusion of ions from core (higher concentration) toward shell (lower concentration) till formation of void based on Kirkendall Effect. **d** SEM image of HA crystals around voids indicating that ACP completely transformed to HA and left void behind. Reprinted with permission from [33]

core, the interface moves toward the shell. Therefore, the vacancies are left behind until they form a void [33]. The diffusion flux of ACP ions from core to shell is calculated according Fick's first law of diffusion.

$$q = -D\frac{\partial C}{\partial x} \tag{10}$$

In which q is diffusion flux (mol.m^{-2} s^{-1}), D is diffusion coefficient (m^2/s), C is concentration (mol/m^3), and X is position (m) [34, 35].

4.4 Spiral growth

The growth process of crystals from solution can be achieved by several cooperative mechanisms. These mechanisms include attachment of molecules onto the surface, diffusion toward active points on the surface, and the detachment at those active points. During this process, growth steps must be produced consistently which are influenced by supersaturation factor in the system. If the driving force is below critical value, intrinsic dislocations become responsible to direct nucleation and growth processes on the surfaces. The stacking faults provide screw dislocations as an endless source upon growth process. This growth preserves first formed stacking fault of the lattice. Particle attachment along screw dislocation leads to the formation of spiral growth hillocks which lead to crystallization growth [35, 36]. The growth rate is given by the equation below.

$$G = k_g(S_a - 1)^g \tag{11}$$

Here G (m/s) is the growth rate, S_a is the activity-based supersaturation ratio, $k_g$is growth rate constant, and g is the growth order at low supersaturation level. When the growth process is dominated by dislocations spirals, value of g is considered [35, 36].

Li et al. showed the morphology evolution during HA surface growth by spiral growth mechanism [37]. They also showed that the aggregation of Posner nanoclusters and pre-nucleation nanoclusters is suggestive of classical crystallization mechanisms such as spiral growth. Based on classical mechanisms, growth of HA nanocrystals occurs by addition of individual ions on crystal surfaces. Incorporation of such these ions inside the crystal structure encounters high energy barrier during growth of HA crystals. The HA solubility is a critical factor in determining the rates of ion-by-ion attachment. In the cases where HA is soluble, spiral

growth mechanism might be energetically favorable for HA crystallization. This then leads to the formation of hexagonal growth hillocks on the (100) surface of HA [37]. Figure 7 shows in situ AFM images of HA formation along (100) face in a supersaturated solution along screw dislocation. In addition, this figure also shows the formation of HA in six unique directions and the velocity of step growth process as a function of different supersaturation values.

4.5 Layer-by-layer growth mechanism

Lotsari et al. investigated a pathway of mineralization on bone-biomimetic polymerized lyotropic liquid crystal (PLLC) [38]. They indicated that ACP clusters form as amorphous granules (d ≈ 50–80 nm). These amorphous clusters transform into thin plate-like crystal HA (50 × 30 × 2 nm^3). ACP to HA transformation initiates by cluster migration with layer-by-layer growth process confined within the spaces of the PLLC matrix, as schematically exhibited in Fig. 8a. The high-resolution TEM images shown in Fig. 8b reveals the continues crystallization of HA within ACP nanoparticle through layer-by-layer mechanism. It also shows the elongation of particle along c-axis of crystalline region due to the difference in density between amorphous and crystalline phases. The nucleation of crystalline phase initiates from confined space of PLLC matrix and growth occurs along c-axis of PLLs fibrils [38].

5 The impact of external factors on biomineralization

5.1 The effect of pH

Conversion rate of ACP to HA can be controlled by pH values between 6.8 and 10 with anions such as carbonate being used [39]. This rate increases as pH value goes up from 7 to 10, and this upward trend is reversed at pH greater than 10. When the pH is close to 9, the ACP to HA transformation proceeds via

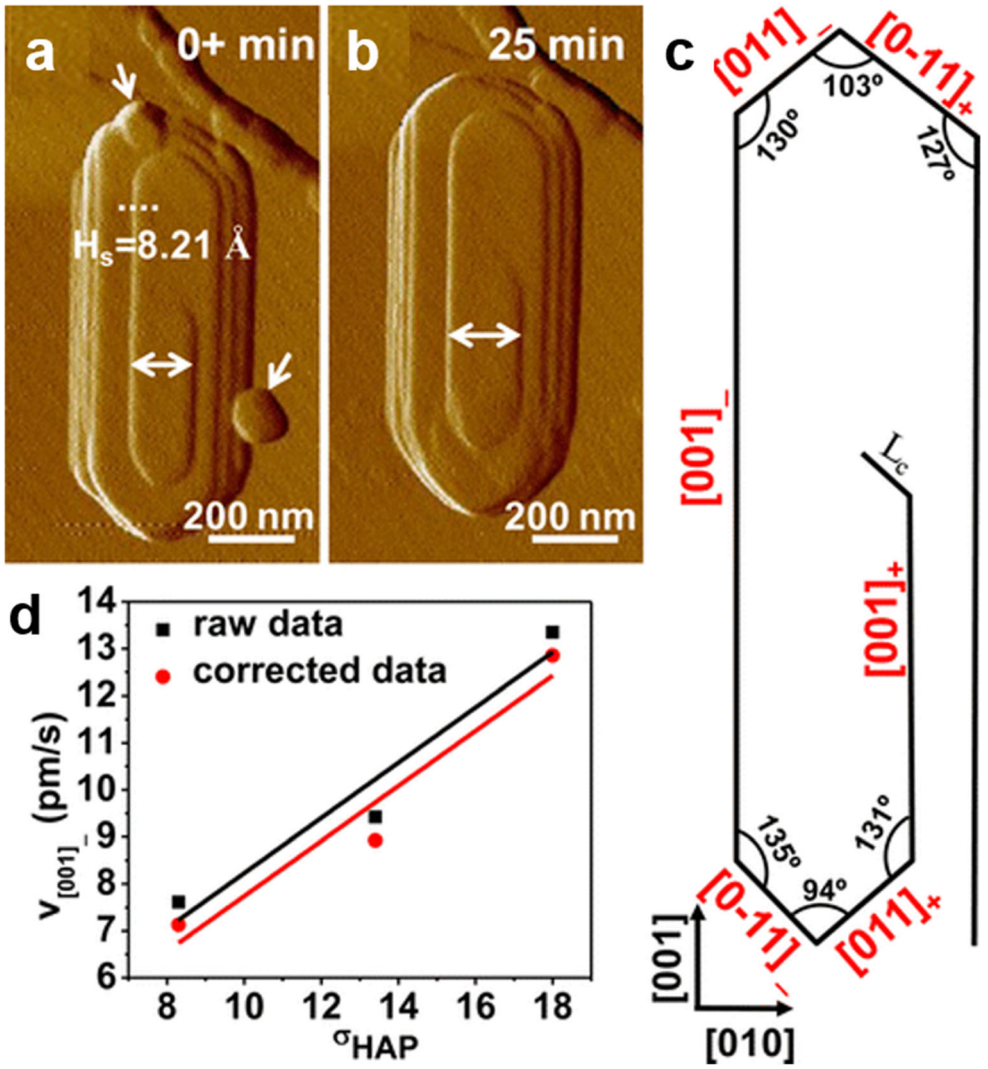

Fig. 7 In situ AFM of growth process of HA along (100) plane. **a, b** Particle attachment along screw dislocation and formation of spiral growth hillock at σ (HA) = 18. White dotted line indicates step height (8.21 Å); arrows show first formed HA particles. **c** Shows six unique directions during growth process of HA in which Lc is critical length of each step. **d** Indicates step growth velocity in the direction of [001] — as a function of supersaturation values. The black and red lines state raw data and corrected data measured by AFM (R2 = 0.89), in sequence. Reprinted with permission from [37]

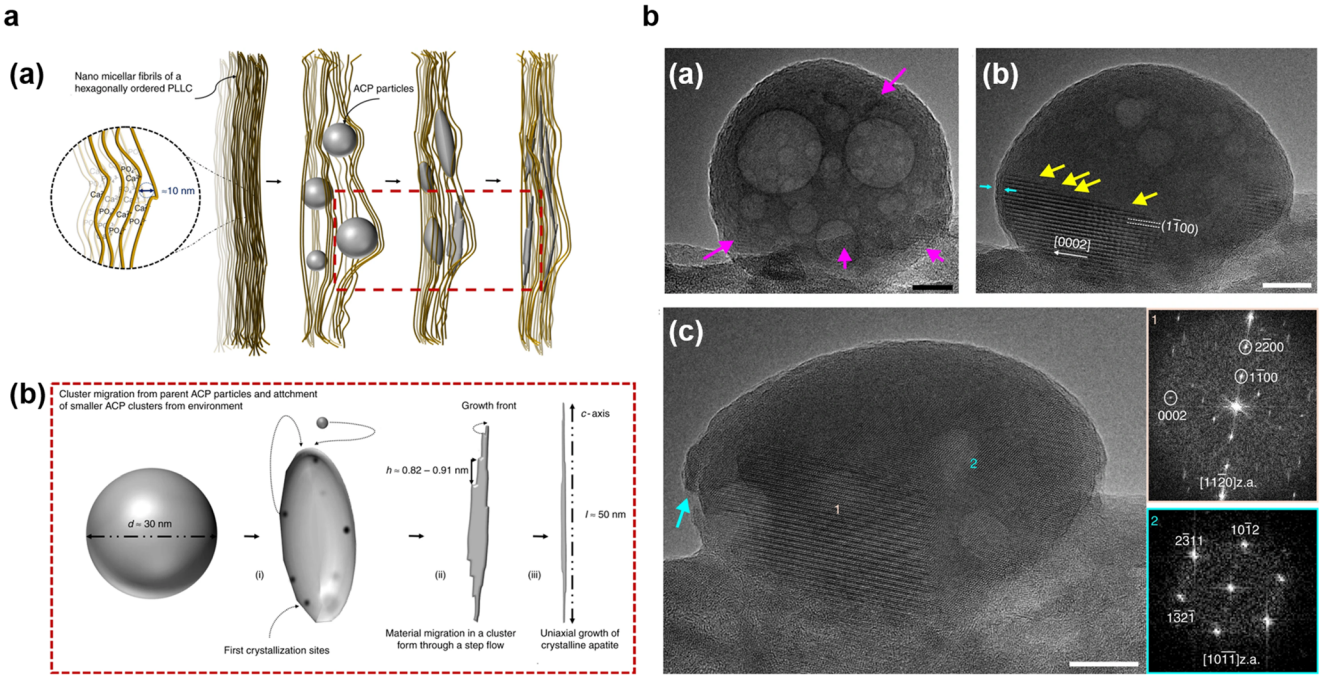

Fig. 8 Transformation of ACP to HA through step growth and layer by layer mechanisms **a.** (a) Schematic shows the pathways of mineralization within PLLC fibrils with interlayer distance of 10 nm. (b) Length of PLLC fibrils. (i) Partially crystallization on the surface of ACP and deformation of ACP along c-axis, (ii) initiating step growth process along c-axis as a result of cluster migration, and (iii) non-uniform growth of HA crystals. **b.** Partially crystallization of ACP nanoparticle via layer-by-layer process. HRTEM images indicate ACP nanoparticle (a) before and (b) after partially crystallization (after 2 min), respectively, as presented by arrows. Blue arrows also represent the thickness of ACP nanoparticle (1.5 nm). (c) HRTEM image shows progressive crystallization and formation of second crystalline region on the surface of ACP after 4 min. FFT diffractograms confirm two formed crystalline regions. Scale bars (a–c) are 10 nm. Reprinted with permission from [38]

the formation of octacalcium phosphate (OCP) as an intermediate metastable phase. Thereafter, plate-like crystals of HA begin nucleating on the surface of OCP. At a pH above 10, the concentration of HPO_4^{-2} ions, a crystallization inhibitor, decreases in the solution, while concentration of $CaPO_4^{-1}$ ions, a crystallization accelerator, causes a calcium ion depletion. This then leads to a reduction in induction time [40]. Figure 9 indicates the impact of different pH values the on concentrations of nucleation and growth units of HA such as HPO_4^{-2} and $CaPO_4^{-1}$. This is further confirmed by work done by Gebauer et al. [41]. Here, the work examined the effect of pH on the binding of calcium ions, a cation, on an electron donor; in this study it was carbonate ion, an anion. The researchers reported that increasing the pH toward alkaline medium could induce calcium binding to carbonate ions. They concluded that increasing pH can induce higher tendency of calcium binding leading to faster pre-nucleation formation. They also noted that the formation of these clusters takes place in both under and supersaturation solutions.

5.2 The effect of additives

Another factor which affects ACP to HA transformation is addition of additives such as ion species of magnesium, fluoride, and silicon [42–44]. Magnesium ions are present in organs such as teeth and bones with the ratio of calcium to magnesium ion mole ratios being from 0.004 to 0.04. To illustrate this, Boskey and Posner revealed that magnesium ion forms stronger bonding with phosphate ions instead of calcium ions [42]. These strong bonds could prevent ACP from dissolution.

Another phosphate mineral, fluorapatite, with empirical formula of $Ca_5(PO_4)_3F$, can be found in dentin and enamel. During formation of fluorapatite, hydroxide present in lattice structure of HA $Ca_5(PO_4)_3OH$, get replaced by fluoride ion, making it less soluble with solubility product value of 8.6 × 10–61 in comparison to HA with a solubility product value of 2.35 × 10–59 in acidic solutions [43]. Fluorapatite also looks different from HA in terms of hardness and shape of crystal. These rod-shaped crystals of fluorapatite are stiffer and harder than plate-shaped crystals of HA. Another example is that ionic silicon also facilitates formation of HA due to the fact that silicon accelerates hydrolysis of ACP leading to formation of HA crystals [43, 44].

6 Collagen

6.1 Structure of collagen I

Collagen is known to be the main member of triple helical proteins with hierarchical structure [44, 45]. This fibrous protein

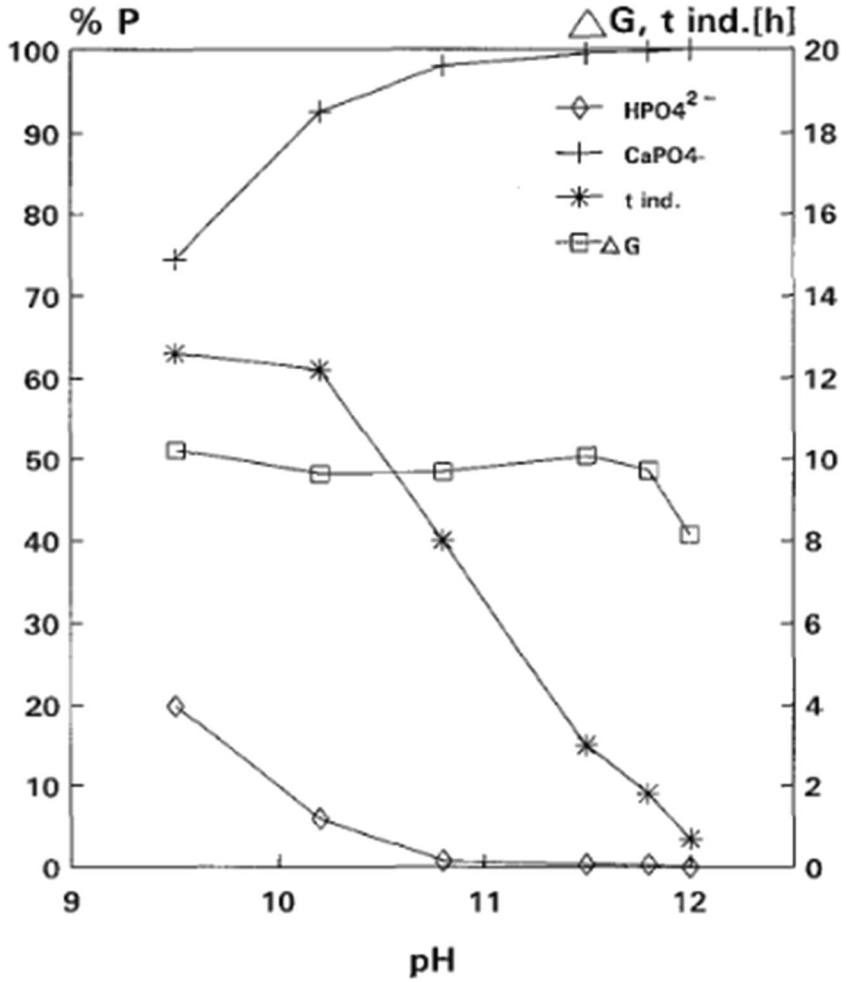

Fig. 9 The impact of pH value on ionic species in the solution, induction time and conversion rate ACP to HA. Reprinted with permission from [24]

consists of three polypeptide chains with the length of ~ 300 nm, each of which has a repeating Gly-X-Y sequence. Glycine, as a small molecule, fits in the center of structure due to hydrogen bonds and different polypeptide chains which helps to hold them together [46]. Glycine actively keeps the collagen unyielding and flexible. Moreover, X and Y are often proline and hydroxyproline which stabilize right-handed triple helical structure which also increases the tensile strength of collagen [47–49].

Each polypeptide is made up of two regions named the N and C terminal propeptides. These two regions are removed upon the conversion of tropocollagen into fibrils [49, 50]. The C and N terminal propeptides restrict lateral growth leading to the formation of narrow fibrils. When the cleavage of both propeptides happens, there is lateral growth which is required for fibrils formation [51, 52]. Tropocollagens are cross-linked via covalent bonds and each one possesses approximately 1000 amino acid residues with the length of roughly 300 nm which five of them form a procollagen [44, 45]. During the formation of procollagen, these five tropocollagens are assembled via a quarter staggered arrangement in which repeated expression of this arrangement in vicinal rows causes to produce a D-periodic structure with a 67-nm repeat [52, 53]. D-period is specific characteristic of collagen which emerges from the repeat of gap zones of 0.6 of period and overlap regions 0.4 of period [47, 54]. Under electron microscopy, as shown in Figure 10a, collagen fibrils exhibit this D-periodic structure in the form of 12 dark lines of which a3, a2, a1, e2, e1, d, and c3 bands are attributed to gap zone. Bands c2, c1, b2, and b1 are assigned to the overlap region, and a4 is known to be in the boundary of both gap zone and overlap region [57–60]. Using TEM, such as in Fig. 10b, it is possible to measure the length of each band. There are two regions that are charged, the c-band and a-band which are near to the N-terminus and the C-terminus of collagen molecule. These regions provide appropriate sites for nucleation of calcium phosphate clusters [2, 47, 60–62].

Xu et al. simulated a collagen structure to clarify the nucleation process of calcium phosphate minerals within fibrils of collagen [55, 62]. They investigate vital role of charged amino acids residues during intrafibrillar mineralization. The model showed that such these charged residues in the collagen molecules are oriented toward the hole zone of collagen and act as

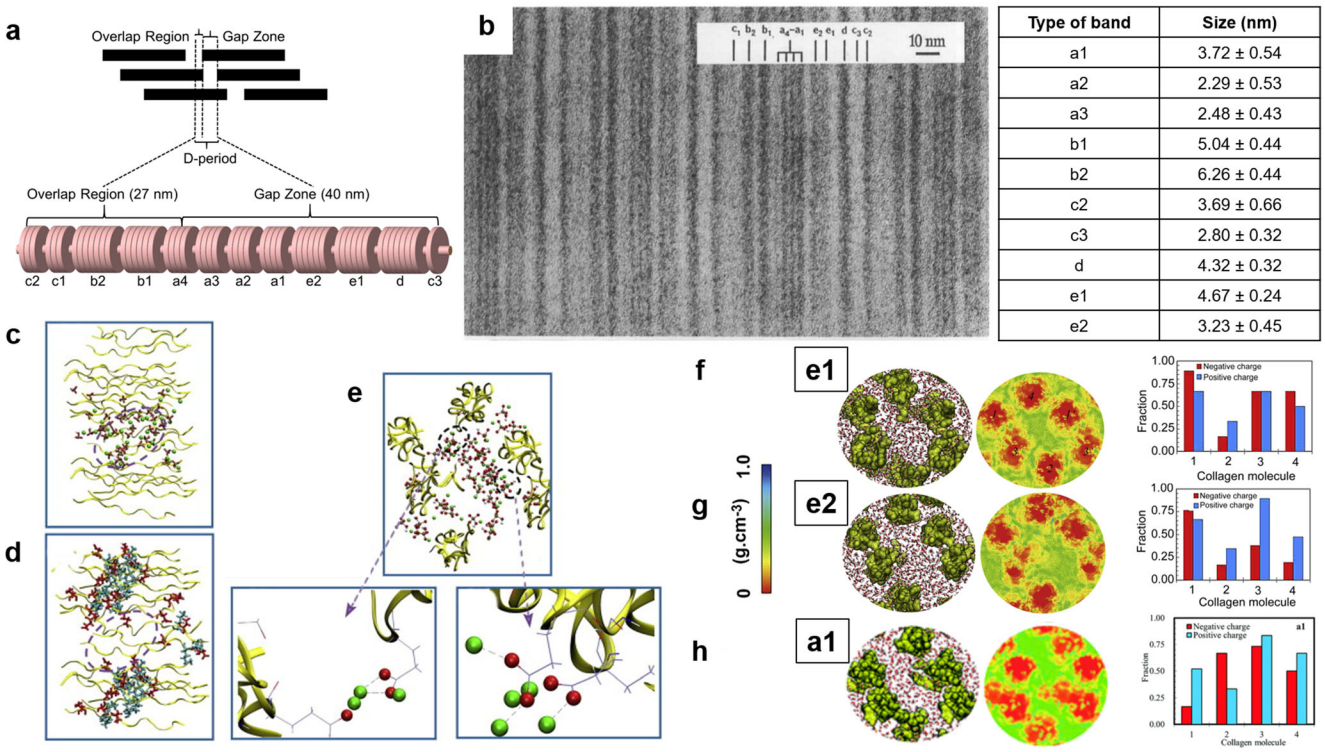

Type of band	Size (nm)
a1	3.72 ± 0.54
a2	2.29 ± 0.53
a3	2.48 ± 0.43
b1	5.04 ± 0.44
b2	6.26 ± 0.44
c2	3.69 ± 0.66
c3	2.80 ± 0.32
d	4.32 ± 0.32
e1	4.67 ± 0.24
e2	3.23 ± 0.45

Fig. 10 The key role of hole zone on collagen biomineralization. **a** D-period is known to be a fingerprint of collagen which consists of two areas, gap zone and overlap region with the lengths of 40 and 27 nm, respectively. Gap zone consisted of different bands containing a3, a2, a1, e2, e1, d and c3; overlap region possesses c2, c1, b2, and b1, and a4 is located at the boundary between gap zone and overlap region. **b** TEM image and table show bands appeared on of stained, non-mineralized collagen and lengths of 12 bands in D-period of collagen measured using Image J, respectively. Reprinted with permission from [47]. **c**–**d** Snapshots of forming salt bridge nests in which collagen molecules, positively, and negatively charged amino acids are shown as yellow ribbons, blue and red molecules. **e** Snapshots of forming Ca-P cluster in the e2 band located at hole zone of collagen where interactions between positively (blue color) and negatively (red color) charged residues occur indicating preferable orientation of Ca-P toward hole zone of collagen especially e1 and e2 bands; Ca, P, and O ions are shown as blue, grey, and red spheres. **f**–**h** The fraction of charged amino acids residues in the hole zone of collagen, distribution of water molecules and density for the bands of e1, e2, and a1, respectively. Reprinted with permission from [55, 56]

template to accommodate ACP with particle sizes ranging from 1.3 to 1.6 nanometers. Most of the calcium and phosphate ions are located in the hole zone of collagen where interactions between amino acid residues take place [55, 63]. Here the e1 and e2 bands could be considered as sites to initiate nucleation of calcium phosphate clusters, Fig. 10 c, d, and e. Additionally, density of water in hole zone of collagen fibrils is 30% is lower than its bulk density of water [55, 62]. The decrease in density could accelerate nucleation in hole zone of collagen by reducing enthalpy cost of dissolution of ions. The molecular dynamics simulations done by Xu et al. show atomic structure of collagen I fibrils to facilitate understanding of mineralization in intrafibrillar of collagen. They found that pseudohexagonal arrangement was maintained in hole zone of collagen which was attributed to the a and e bands and distorted the transition area between overlap region and gap zone of the d and c3 bands. The hole zone forms a preferred direction of charged amino acid residues to accelerate diffusion of calcium phosphate species and act as initial sites of nucleation. However, diffusion of minerals is slow in distorted area due to tortuosity of pathway as compared to ideal pathways in a and e bands. These transition regions could also provide secondary sites of nucleation. Moreover, Xu et al. suggested that 70% of the charged residues are located at hole zone of collagen around e bands. All the bands located at hole zone including a and e bands can provide appropriate sites for diffusion of calcium phosphate clusters within fibrils of collagen. With only fraction of charged amino acids being available and the distribution of water density, the e bands are most favorable for infiltration of calcium phosphate species, as shown in Fig. 10 f, g, and h [56].

Proteoglycans are proteins that have polyanionic domains which accommodate phosphate and polycarboxylic acid functions. Proteoglycans are able to control collagen biomineralization in three ways. First, these proteins can inhibit lateral growth and deformation of collagen fibrils through interfering with their interactions. Second, by interaction with charged amino acid residues, proteoglycans occupy gap zone of

collagen fibril by which it could hamper calcification. Finally, proteoglycans could inhibit mineral formation in the external space of collagen [51].

6.2 Collagen biomineralization

The term collagen biomineralization refers to the deposition of minerals in intrafibrillar of collagen until formed crystals reach required geometry for strengthening collagen [56, 64]. Pathological biomineralization can also occur outside collagen fibrils; such formation outside the collagen fibrils is known as extrafibrillar mineralization [65]. In order to understand aberrant biomineralization, it is crucial to understand the mechanisms by which collagen is mineralized and the related pathways. Structurally, there is evidence of extrafibrillar and hierarchical mineralization. The work of Reznikov et al. provided insight into the 3D structural organization and the hierarchy of the bone mineralization by nanoscale structural characterization [66]. The authors leveraged high-resolution transmission electron microscopy and crystallographic data together with tomographic imaging to construct a 3D model of bone mineral and its organic matrix. The results showed the presence of three different mineral structural motifs: filamentous, lacy, and rosette corresponding to in-plane or longitudinal, out-of-plane, and hexagonal crystal structure. Furthermore, the data revealed the following hierarchy of the apatite crystals: needle- and plate-like nanocrystals that laterally arrange into platelets, which in turn form stacks of platelets. These structures, together with acicular crystals, form large polycrystalline structures that span across fibrils. The significance of these findings includes identifying the cross-fibrillar nature of mineralization, with helical pattern in the 3D bone structure. Similarly, Schwarcz et al. used dark field TEM to identify extrafibrillar mineral structures of elongated plates surrounding and parallel to collagen fibrils [67]. These structures were found to contain individual apatite crystals, with ~ 1 nm spacing between plates, and provide evidence for mineral formation outside of fibrils.

The mineralization can be either undesirable or desirable for mineral formation in extrafibrillar and intrafibrillar spaces of collagen fibrils, respectively [68]. In intrafibrillar mineralization, the mineral components form within a hydrated matrix of macromolecules which is very rich in biopolymers associated with positively and negatively charged groups such as polysaccharides [69]. These macromolecules play vital role during mineralization in collage fibrils by stabilizing calcium phosphate precursors which transform into amorphous phase followed by HA crystal formation. They are also known as nucleation inhibitors in extrafibrillar space of collagen. Smeets et al. showed that such polysaccharides bind to calcium ions and concentrate them [70]. Not only polysaccharides decrease calcium ions in the solution by creating high local supersaturation, but they also avoid immediate formation of vaterite due to lack of calcium and carbonate ions.

Collagen is associated with proteoglycan-rich protein and non-collagenous protein in the extracellular matrix. These proteins can act as a template to induce biomineralization via directing oriented nucleation of HA crystals. It also provides a confined space for growth of HA crystals along c-axis of collagen fibrils [71]. Nudelman et al. studied role of collagen during mineral formation at the microscopic scale using cryogenic TEM. They employed polyaspartic acid (PAsp) and fetuin to biologically mimic non-collagenous proteins. PAsp and fetuin are added in order to stabilize PNCs particle size and chemical interactions. These stabilized clusters are loosely packed and infiltrate the collagen fibrils. Nudelman et al. also demonstrated that collagen actively provide specific sites, a-bands, for loosely packed calcium phosphate clusters to infiltrate through electrostatic forces between collagen fibrils. The calcium phosphate clusters uniformly nucleate and grow throughout gap zone and overlap region, particularly in d band located at gap zone of collagen. Therefore, it could be concluded that collagen is able to actively govern mineralization in absence of any nucleation inhibitor. Calcium phosphate clusters can move toward the a-bands to reach intrafibrillar space of collagen and HA crystals form at the expense of ACP clusters [73]. In another study, Wang el al. reported that collagen affects HA crystals in terms of both structural features at microscopic scale e and geometrical dimensions at macroscopic scale [71]. In the former, collagen influences the structure of phosphate ions in HA crystals and intrafibrillar water.

There are two pathways by which mineralization could possibly take place, intrafibrillar mineralization or extrafibrillar mineralization. Kim et al. analyzed the pathways through calcium phosphate clusters nucleate and grow within collagen intrafibrillar using in situ small angle X-ray scattering [65]. They also examined the role of PAsp as nucleation inhibitor in directing collagen biomineralization. They found that in the absence of PAsp, biomineralization begins with the formation of some spherical ACP in the extrafibrillar spaces of collagen. These aggregates crystalize on the external surfaces of collagen preventing diffusion of free calcium phosphate clusters in intrafibrillar space of collagen, as shown in Fig. 11c. Extracellular mineralization starts with the bonding between free calcium ions in the solution and aggregated ACP clusters [65, 75]. Extracellular mineralization is limited once calcium is stabilized by PAsp and mineralization takes place inside collagen fibrils, shown in Fig. 11c. It was suggested that not only are the pathways are different but also the mechanisms of mineral formation in intrafibrillar mineralization and extrafibrillar mineralization are different [65]. In intrafibrillar mineralization, PNCs directly transform into plate-shaped HA crystals, approximately 1.5 nm in thickness and 40 nm in diameter, without existence of any intermediate phase. Due

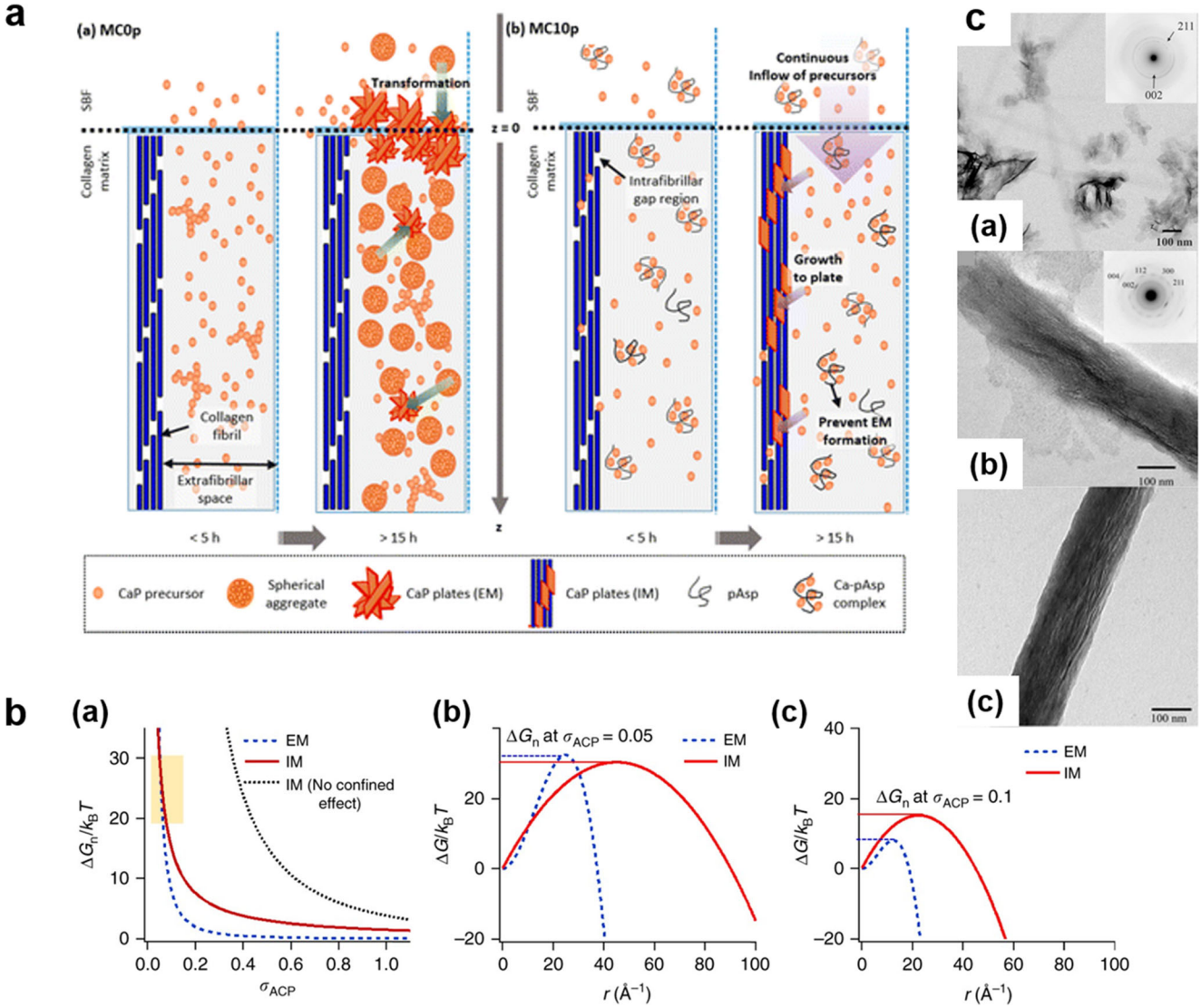

Fig. 11 **a** Mechanisms and pathways of collagen mineralization in (a) presence of PAsp and (b) in the absence of PAsp as nucleation inhibitor. Reprinted with permission from [65]. **b** Changes of energy barrier ΔG_n at various supersaturation values (σ). (a) Changes in ΔG_n for three different proposed nucleation models including IM in the presence of PAsp, EM in the presence and absence of PAsp. (b, c) The differences in value of ΔG_n at σ_ACP = 0.05 and 1 as shown in yellow box. Reprinted with permission from [68]. **c** TEM images and SAED patterns of (a) mineral formation in the absence of PAsp, (b) mineralized collagen after 2 h of incubation, ACP clusters are directed to infiltrate into collagen fibrils, and (c) mineralized collagen after 16 h of incubation, HA crystals form in the length of collagen. Reprinted with permission from [74]

to vital role of PAsp as nucleation inhibitor, the nucleation of HA is slower in extrafibrillar mineralization [65]. In another study, Kim et al. proposed that the differences in nucleation pathways for intrafibrillar mineralization and extrafibrillar mineralization could be explained by their total free energy [68]. They applied in situ X-ray scattering and compared the energy barrier of nucleation between intrafibrillar mineralization and extrafibrillar mineralization. They suggested that PAsp avoids extrafibrillar mineralization through increasing surface energy between ACP and the mineralization solution. The small spacing of collagen provides appropriate sites for nucleation by minimizing interfacial energy value, α, leading to formation HA crystals with two-dimensional morphology and structure, the intrafibrillar mineralization pathway. However, α for intrafibrillar mineralization is 19 ± 1 mJ/m^2 is higher than that of extrafibrillar mineralization 5 ± 1 mJ/m^2 with respect to ACP. Although α and ΔG_n for nucleation of ACP are higher for intrafibrillar mineralization than extrafibrillar mineralization upon the extensive range of supersaturation value, σ_{ACP} ranging between 0.1 and 1.13, as σ_{ACP} decreases to below 0.05, ΔG_n for intrafibrillar mineralization becomes lower than that of extrafibrillar mineralization, as shown in Eq. 12. If σ is less than 0.05, the intrafibrillar mineralization pathway is more favorable for nucleation of

ACP, as shown in Fig. 11 [68].

$$\frac{\Delta G_{n,IM}}{\Delta G_{n,EM}} = \frac{3hK_BT\alpha_{IM}^2}{16\pi v_m T\alpha_{EM}^3}\sigma = 18.8\sigma \quad (12)$$

Here $\Delta G_{n,\ IM}$ and $\Delta G_{n,\ EM}$ stand for nucleation energy barrier for intrafibrillar mineralization and extrafibrillar mineralization, respectively. α_{IM}^2 and α_{EM}^2 represents interfacial energy for intrafibrillar mineralization and extrafibrillar mineralization, respectively. Finally, h is the height of the nuclei.

Using TEM and electron diffraction, Deshpande et al. investigated the impact of PAsp and collagen on bio-inspired mineralization [74]. They observed formation of ribbon-like HA crystals along c-axis of collagen fibrils which resemble HA formed in bone and dentin. Unlike previous studies, they suggested that collagen is not individually able to direct IM and the interactions between PAsp and collagen fibrils are strongly involved during mineralization, as shown in Fig. 11.

7 Phosphate deposited within collagen fibrils

Since collagen is a complex structure, with its multiple regions and long length, the study of phosphate deposition is not limited to just in vivo studies. Rather, in vitro studies are also included to augment our knowledge of the deposition process. Since the perspective of this review is from a materials engineering viewpoint of a process within a biological system, the in vitro studies outlined here are meant to augment the view of the mechanism rather than provide an in-depth perspective of the cellular behavior.

There are several hypotheses by which calcium phosphate minerals are deposited inside collagen fibrils including polymer-induced liquid-precursor, cell-controlled mechanism, dissolution-precipitation, and electrostatic forces [76–79]. Olszta et al. hypothesized that intrafibrillar mineralization may happen through polymer-induced liquid-precursor . Based on this hypothesis, PAsp chains sequesters calcium ions, while inhibiting extrafibrillar mineralization, to induce liquid-liquid phase separation in the buffered solution leading to form droplets of hydrated ACP. These hydrated ACP clusters are drawn into hole zone of collagen fibrils through capillary action. The collagen fibrils are swollen with droplets and replace the intrafibrillar water. Then ACP clusters crystalize into HA nanocrystals along c-axis of collagen fibrils as seen in Fig. 12b–c.

Biomineralization could also proceed by a couple of cell-controlled cooperative mechanisms [76]. There are three proposed mechanisms for cell-controlled biomineralization. First, matrix vesicles budded from the plasma membrane concentrate calcium and phosphate ions in extracellular space prior to mineralization within collagen. Second, non-collagenous proteins coupled with intrafibrillar of collagen mediate mineral nucleation within collagen fibrils. Third, ACP and ionic calcium-containing mitochondria are responsible for transport of ACP and calcium ions toward intracellular vesicles. Finally, vesicles accumulate them in the ECM prior to crystallization.

Boonrungsiman at al. proposed a model for dissolution-precipitation [76]. First, vesicles accumulate calcium and phosphate ions in extracellular spaces. Second, they mediate precipitation of calcium phosphate or ACP clusters extracellularly. Finally, they disperse the clusters on the ECM. The mitochondria accommodate clusters as granules in intracellular spaces. The clusters are then transported from mitochondria toward intracellular vesicles via diffusion. Figure 12e shows how a calcium phosphate containing vesicle inside osteoblast cells embedded within ECM promotes the formation of ACP inside vesicles. They accumulate ACP particles in extracellular spaces on the surface of collagen and eventually mediate ACP to HA transformation in extrafibrillar of collagen along the 002, 112, 211, and 300 planes. The transportation process of intravascular ACP from the intracellular to extracellular spaces was verified by Mahamid et al.'s study [78]. The study was done on the formation of mouse calvaria and long bones. They showed that bone cells accumulate membrane-bound mineral granules within intracellular vesicles. These granules are made of disordered calcium phosphate as main precursor of more stable phase. The intracellular mineral consists of significantly less calcium to phosphate ratio which first formed phosphate entities isolate the calcium ions within intracellular vesicles. These polyphosphates can form strong covalent bonds with calcium ions leading to high local supersaturation of both calcium and phosphate ions. Bone cells such as pre-osteoblasts, osteoblasts, and osteocytes are able to actively generate disordered mineral granules within intracellular vesicles. Afterward, osteoblast cells induce mineralization by creating reservoirs to transport minerals, 80 nm granules, into the extracellular space. In vivo bone cells also accumulate ACP phase within intracellular vesicles that have a low calcium to phosphate ratio. These cells are able to induce precipitation of initial mineral phase in extrafibrillar space of collagen during mineralization process.

Recently, Mahamid et al. investigated biomineralization inside zebrafish fin rays [82]. They found that ACP is the major component in the formation of fin bones. Under in vitro conditions of neutral pH and ACP supersaturation, ACP converts to octacalcium phosphate (OCP). OCP then transforms into a more thermodynamically stable compound, HA. The HA nanocrystals grow in the hole zone of collagen along is c-axis. Similarly, Wang et al. observed small amount of ACP nanoparticles in mature baboon bone [83]. They also showed that there are two pathways by which ACP phase could play a role in collagen biomineralization. First, ACP nanoparticles might be directly deposited inside collagen

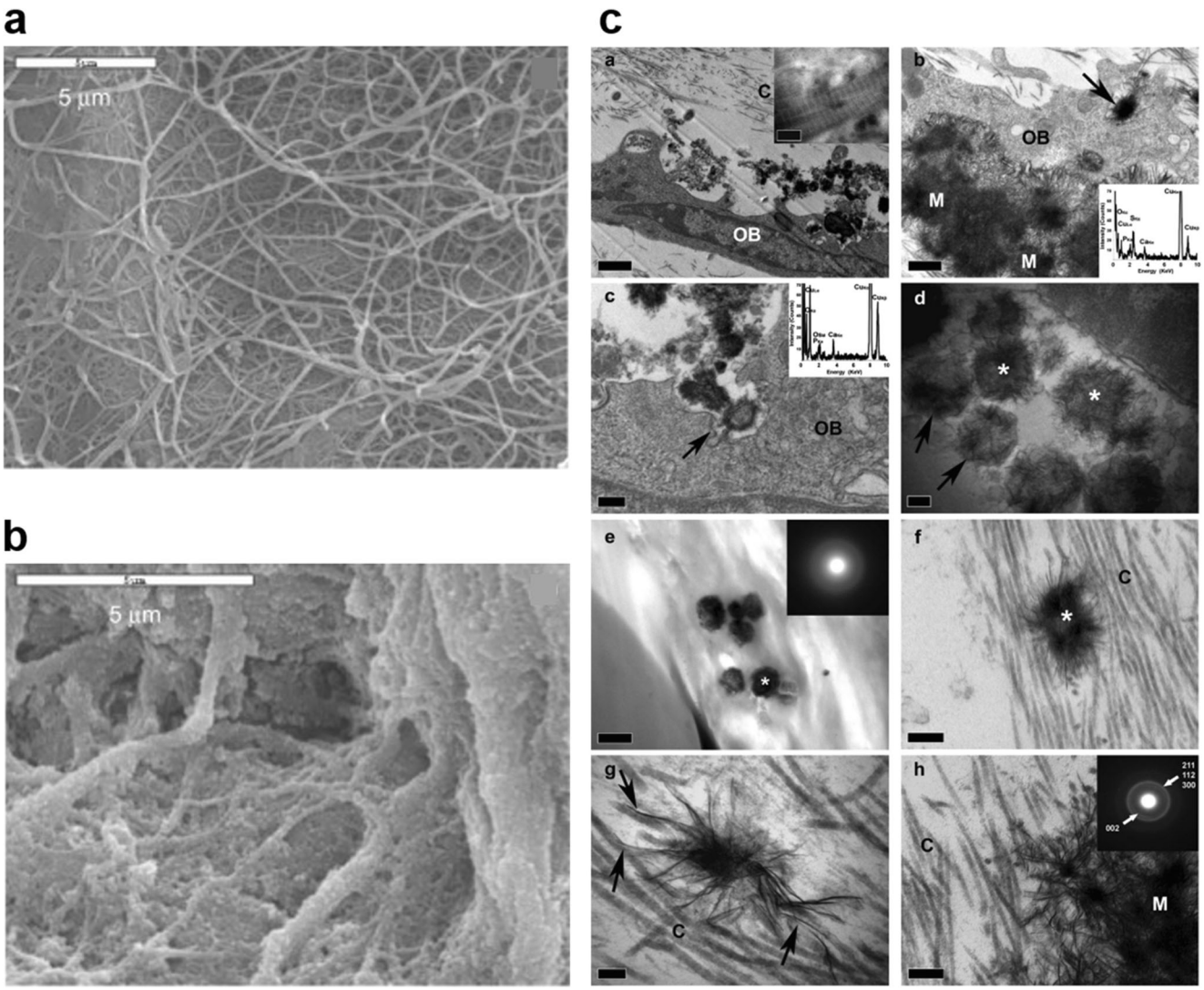

Fig. 12 **a** Non-mineralized collagen and **b** mineralized collagen in the presence of polyaspartate after 4 days of induction. Reprinted with permission from [79]. **c** Bright-field TEM images of bone cell-controlled biomineralization, (a) osteoblast (OB) cell located within extracellular matrix (ECM). (b) Calcium phosphate containing vesicle (arrow) located at osteoblast cells are embedded within mineralized nodules (scale bar, 0.5 μm). (c) The presence of vesicles consisting of calcium and phosphate ions intracellularly (scale bar, 0.2 μm). (d) Calcium phosphate containing vesicles in extracellular spaces neighboring an osteoblast cell (scale bar, 0.2 μm). (e) Aggregations of calcium phosphate in a mineralized nodule-like area (scale bar, 0.5 μm). (f) Accumulation of calcium phosphate aggregations in extrafibrillar of collagen (scale bar, 0.2 μm). (g) Emanating mineral (arrow) in extrafibrillar space of collagen (scale bar, 0.2 μm). (h) Biomineralization on the surface of collagen fibrils (scale bar, 0.2 μm). Reprinted with permission from [76]

fibrils and transform to crystalline phase. Second, ACP nanoparticles form in the extrafibrillar space of collagen by penetrating the gap zone of collagen and transforming into HA phase.

Kerschnitzki et al. studied biomineralization pathway of long bones of the chicken embryo [84]. They observed that osteoblasts precipitate new bone at the periosteal membrane and osteoclasts resorb into the newly formed bone at the endosteal membrane. The bone resorption takes place by acidifying the initially formed bone area and degradation of the collagenous matrix of bone. The vascular system includes blood vessels, osteoclasts, and osteoblasts and is a key system when the bone is degraded. The system is responsible for facilitating the transportation of the components required for mineral formation to the new bone precipitation site. The amounts of ions that can be transported are restricted by the low solubility of bone mineral at neutral pH. Osteoclasts are reservoirs of resorbed minerals, mostly in mitochondrial units and intracellular vesicles. The transportation of the minerals occurs to the extrafibrillar of collagen where they are not bounded to membrane. Moreover, because bone mineral is stored in the form of membrane-bound particles, the danger caused by calcification of ectopic vascular is minimized. A similar observation was noted in the tail fin tissue of larval zebrafish [82–85].

On the other hand, Nudelman et al. proposed that calcium and phosphate ions could infiltrate into collagen fibrils through dissolution-precipitation mechanism [3]. ACP clusters dissolve in the solution and ions diffuse into intrafibrillar of collagen. Subsequently, they nucleate in the hole zone of collagen and grow along collagen fibril. Nudelman et al. suggested that ACP could enter the collagen fibrils via electrostatic interactions between positively charged sites present in the hole zone of collagen and negatively charged PAsp-calcium phosphate complexes. Polyallylamine hydrochloride (PAH), as a polycation, could also inhibit aggregation of calcium phosphate ions in the solution [80]. Niu et al. developed PAH-controlled intrafibrillar mineralization study that examined the previous model based on which short-ranged electrostatic interaction is likely involved in polyelectrolyte-directed intrafibrillar mineralization [80]. The data suggested that regardless of what type of charge polyelectrolyte has in the solution, ions and water move out from intrafibrillar spaces of collagen leading to shrinkage of collagen fibrils. Moreover, shrinkage of fibrils caused a concentration gradient of ions and PNCs toward intrafibrillar space of collagen. In the polycation system, PAH molecules bind to carboxyl group of collagen fibril inducing positive charge on the collagen surfaces. The system caused the number of available carboxyl group to decrease while increasing the number of amine ones. Consequently, coulomb forces short range interaction was limited between PAH-ACP complexes and bands of collagen. Thus, long distance interactions were proposed as a possibility to promote intrafibrillar mineralization in an electrolyte system. Also, collagen membrane is selectively permeable. With PAH having a molecular weight of 15 kDa and PAsp having a molecular weight of 27 kDa, only long-distance interaction might be involved upon intrafibrillar mineralization.

While significant work has been done to understand pathways of collagen biomineralization, the contribution of collagen-cross linked nucleation inhibitor has not been as well investigated [81]. Surface modifications of collagen raise the number of carboxylate groups leading to accelerate collagen biomineralization [86]. Song et al. applied negatively charged polyacrylic acid with high molecular weight in a solution containing reconstituted collagen in order to develop collagen-bound ligands [81]. Cryogenic electron microscopy and molecular dynamics simulation demonstrated that collagen-ligand interactions promote and accumulate aggregation of PNCs. The PNCs form a chain-like structure in intrafibrillar space of collagen leading to intrafibrillar mineralization along the c-axis of collagen fibrils. Cryogenic electron microscopy images indicate that the concentration of ACP and PNCs aggregates along the surface of collagen in both bare collagen and PAA-bound collagen as seen in Fig. 12 h, i, and j. The presence of ligands on the surface of collagen leads to mineralized collagen with better of mechanical properties versus mineralized collagen in an aqueous environment [81]. Wang et al. developed collagen-bound peptides to investigate how these immobilized peptides could promote mineralization in collagen fibrils [86]. They found that the peptides that attached to the fibrils of the collagen can induce a more ordered structure to mediate mineralization along c-axis of fibrils and accelerate conversion of minerals into HA crystals.

The size of ACP is important upon mineralization with smaller size of loosely aggregations of ACP supporting faster infiltration and HA crystals formation [87]. In addition, the size of polyanion and polycation molecules could affect mineral infiltration and HA formation inside collagen fibrils. Niu et al. demonstrated that molecules such as fetuin which are known to be larger than 40 kDa are not able to enter the collage fibrils [80]. These large molecules indirectly control mineralization of collagen, while smaller molecules (< 6 kDa) such as spermine and citric acid could freely penetrate collagen fibrils. The presence of the small biomolecules directly controls mineralization via binding to hole zone of collagen. These phenomena could be due to collagen having a size-exclusion feature. Both PAsp and PAH are partially excluded from intrafibrillar of collagen and can promote intrafibrillar mineralization. PAsp with high molecular weight leads to induce higher inhibitory effect and formation of smaller ACP nanoclusters [3].

8 Conclusion

Reviewing in vitro models provides new insights in better understanding of pathways and thermodynamics of mineral formation in bone and dentin. Though they do not prove how mineral infiltrate into fibrils of collagen, there are at least a few hypotheses that justify further research. Generally, the collagen biomineralization is initiated by the penetration of pre-nucleation clusters into the fibrils of collagen. It can be influenced by numerous parameters such as particle size of pre-nucleation clusters, their stability, and interactions with collagen fibrils. Non-collagenous protein, as nucleation inhibitor in extrafibrillar of collagen, stabilizes pre-nucleation clusters in the buffer solution by forming complexes consisting of both pre-nucleation clusters and non-collagenous proteins. Afterward, these formed complexes are directed toward hole zone of collagen fibrils. Collagen can then provide appropriate sites for mineralization inside intrafibrillar in a preferred orientation. Numerous positively charged C-terminal ends of the collagen molecules, in gap zone and the overlap region, attract negatively charged PNCs-NCPs complexes via electrostatic forces. Pre-nucleation clusters thermodynamically seek nucleation sites to reduce energy barrier such as those located at the hole zone of collagen. Consequently, they transform to hydroxyapatite crystals as more stable phase without the existence of any intermediate phase.

Funding R Shahbazian-Yassar acknowledges the financial support from the National Science Foundation (NSF) Division of Materials Research (DMR) Award No. 1710049. T Shokuhfar's efforts are supported by NSF-CBET Award No. 1803693.

References

1. A. Navrotsky, *Energetic clues to pathways to biomineralization: precursors, clusters, and nanoparticles*. Proc Natl Acad Sci U S A **101**(33), 12096–12101 (2004)
2. W. Traub, T. Arad, S. Weiner, *Origin of mineral crystal growth in collagen fibrils*. Matrix **12**(4), 251–255 (1992)
3. F. Nudelman, A.J. Lausch, N.A.J.M. Sommerdijk, E.D. Sone, *In vitro models of collagen biomineralization*. J Struct Biol **183**(2), 258–269 (2013)
4. X. Wang et al., *Biomineralization of calcium phosphate revealed by in situ liquid-phase electron microscopy*. Communications Chemistry **1**(1), 1–7 (2018)
5. E. A. Zimmermann, et al., *Intrinsic mechanical behavior of femoral cortical bone in young, osteoporotic and bisphosphonate - treated individuals in low-and high energy fracture conditions.* Scientific reports **6**(1), 1-12 (2016)
6. D. Zahn, *Thermodynamics and kinetics of prenucleation clusters, classical and non-classical nucleation*. ChemPhysChem **16**(10), 2069–2075 (2015)
7. P.G. Vekilov, *The two-step mechanism of nucleation of crystals in solution*. Nanoscale **2**(11), 2346–2357 (2010)
8. J.W. Gibbs, *On the equilibrium of heterogeneous substances.* 1879.
9. S. Karthika, T. Radhakrishnan, P. Kalaichelvi, *A review of classical and nonclassical nucleation theories*. Cryst Growth Des **16**(11), 6663–6681 (2016)
10. F. Bakhtar et al., *Classical nucleation theory and its application to condensing steam flow calculations*. Proc Inst Mech Eng C J Mech Eng Sci **219**(12), 1315–1333 (2005)
11. D. Gebauer, H. Cölfen, *Prenucleation clusters and non-classical nucleation*. Nano Today **6**(6), 564–584 (2011)
12. J. Harding, C. Freeman, D. Duffy, *Oriented crystal growth on organic monolayers*. CrystEngComm **16**(8), 1430–1438 (2014)
13. T.H. Zhang, X.Y. Liu, *How does a transient amorphous precursor template crystallization*. J Am Chem Soc **129**(44), 13520–13526 (2007)
14. W.J. Habraken et al., *Ion-association complexes unite classical and non-classical theories for the biomimetic nucleation of calcium phosphate*. Nat Commun **4**(1), 1–12 (2013)
15. D. Gebauer, M. Kellermeier, J.D. Gale, L. Bergström, H. Cölfen, *Pre-nucleation clusters as solute precursors in crystallisation*. Chem Soc Rev **43**(7), 2348–2371 (2014)
16. N.C. Blumenthal, A.S. Posner, *Hydroxyapatite: mechanism of formation and properties*. Calcif Tissue Res **13**(1), 235–243 (1973)
17. H. Kun et al., *Revealing nanoscale mineralization pathways of hydroxyapatite using in situ liquid cell transmission electron microscopy.* Science Advances **6**(47), eaaz7524 (2020)
18. S. Kim, H.S. Ryu, H.S. Jung, K.S. Hong, *Influence of Ca/P ratios of starting solutions on the crystallization of amorphous calcium phosphate to hydroxyapatite*. Met Mater Int **10**(2), 171–175 (2004)
19. K. Onuma, A. Ito, *Cluster growth model for hydroxyapatite*. Chem Mater **10**(11), 3346–3351 (1998)
20. L. Wang, G.H. Nancollas, *Calcium orthophosphates: crystallization and dissolution*. Chem Rev **108**(11), 4628–4669 (2008)
21. V. Uskoković, S. Tang, V.M. Wu, *On grounds of the memory effect in amorphous and crystalline apatite: kinetics of crystallization and biological response*. ACS Appl Mater Interfaces **10**(17), 14491–14508 (2018)
22. W. Zhao, Z. Xu, Y. Yang, N. Sahai, *Surface energetics of the hydroxyapatite nanocrystal–water interface: a molecular dynamics study*. Langmuir **30**(44), 13283–13292 (2014)
23. M. Tung, W. Brown, *An intermediate state in hydrolysis of amorphous calcium phosphate*. Calcif Tissue Int **35**(1), 783–790 (1983)
24. S. Lazić, *Microcrystalline hydroxyapatite formation from alkaline solutions*. J Cryst Growth **147**(1-2), 147–154 (1995)
25. V. West, *Observations on phase transformation of a precipitated calcium phosphate*. Calcif Tissue Res **7**(1), 212–219 (1971)
26. F. Abbona, A. Baronnet, *A XRD and TEM study on the transformation of amorphous calcium phosphate in the presence of magnesium*. J Cryst Growth **165**(1-2), 98–105 (1996)
27. S. Kim, H.S. Ryu, H. Shin, H.S. Jung, K.S. Hong, *In situ observation of hydroxyapatite nanocrystal formation from amorphous calcium phosphate in calcium-rich solutions*. Mater Chem Phys **91**(2-3), 500–506 (2005)
28. K. Onuma, A. Oyane, K. Tsutsui, K. Tanaka, G. Treboux, N. Kanzaki, A. Ito, *Precipitation kinetics of hydroxyapatite revealed by the continuous-angle laser light-scattering technique*. J Phys Chem B **104**(45), 10563–10568 (2000)
29. S. Somrani, M. Banu, M. Jemal, C. Rey, *Physico-chemical and thermochemical studies of the hydrolytic conversion of amorphous tricalcium phosphate into apatite*. J Solid State Chem **178**(5), 1337–1348 (2005)
30. S.V. Dorozhkin, *Amorphous calcium (ortho) phosphates*. Acta Biomater **6**(12), 4457–4475 (2010)
31. E. Kirkendall, *Rates of diffusion of copper and zinc in alpha brass*. Trans AIME **133**, 186–203 (1939)
32. H. Nakajima, *The discovery and acceptance of the Kirkendall effect: the result of a short research career*. JoM **49**(6), 15–19 (1997)
33. J. Tao, H. Pan, J. Wang, J. Wu, B. Wang, X. Xu, R. Tang, *Evolution of amorphous calcium phosphate to hydroxyapatite probed by gold nanoparticles*. J Phys Chem C **112**(38), 14929–14933 (2008)
34. F. Wang, V.N. Richards, S.P. Shields, W.E. Buhro, *Kinetics and mechanisms of aggregative nanocrystal growth*. Chem Mater **26**(1), 5–21 (2014)
35. A. Fick, *Die medizinische physik*. 1858: Vieweg.
36. A.E. Van Driessche, et al., *New perspectives on mineral nucleation and growth: from solution precursors to solid materials*. 2016: Springer.
37. M. Li, L. Wang, W. Zhang, C.V. Putnis, A. Putnis, *Direct observation of spiral growth, particle attachment, and morphology evolution of hydroxyapatite*. Cryst Growth Des **16**(8), 4509–4518 (2016)
38. A. Lotsari et al., *Transformation of amorphous calcium phosphate to bone-like apatite*. Nat Commun **9**(1), 1–11 (2018)
39. A.L. Boskey, A.S. Posner, *Conversion of amorphous calcium phosphate to microcrystalline hydroxyapatite. A pH-dependent, solution-mediated, solid-solid conversion*. J Phys Chem **77**(19), 2313–2317 (1973)
40. Y.K. Kim, L.S. Gu, T.E. Bryan, J.R. Kim, L. Chen, Y. Liu, J.C. Yoon, L. Breschi, D.H. Pashley, F.R. Tay, *Mineralisation of reconstituted collagen using polyvinylphosphonic acid/polyacrylic acid templating matrix protein analogues in the presence of calcium, phosphate and hydroxyl ions*. Biomaterials **31**(25), 6618–6627 (2010)
41. D. Gebauer, A. Völkel, H. Cölfen, *Stable prenucleation calcium carbonate clusters*. Science **322**(5909), 1819–1822 (2008)
42. A. Boskey, A. Posner, *Magnesium stabilization of amorphous calcium phosphate: a kinetic study*. Mater Res Bull **9**(7), 907–916 (1974)
43. N. Saxena, M.A. Cremer, E.S. Dolling, H. Nurrohman, S. Habelitz, G.W. Marshall, L.B. Gower, *Influence of fluoride on the mineralization of collagen via the polymer-induced liquid-precursor (PILP) process*. Dent Mater **34**(9), 1378–1390 (2018)

44. M. Roozbahani, M. Alehosseini, M. Kharaziha, R. Emadi, *Nano-calcium phosphate bone cement based on Si-stabilized α-tricalcium phosphate with improved mechanical properties*. Mater Sci Eng C **81**, 532–541 (2017)
45. T.J. Wess, *Collagen fibril form and function*, in *Advances in protein chemistry*. Elsevier, 341–374 (2005)
46. E.G. Canty, K.E. Kadler, *Procollagen trafficking, processing and fibrillogenesis*. J Cell Sci **118**(7), 1341–1353 (2005)
47. J.A. Chapman, M. Tzaphlidou, K.M. Meek, K.E. Kadler, *The collagen fibril—a model system for studying the staining and fixation of a protein*. Electron microscopy reviews **3**(1), 143–182 (1990)
48. D.J. Hulmes, *Building collagen molecules, fibrils, and suprafibrillar structures*. J Struct Biol **137**(1-2), 2–10 (2002)
49. F.H. Silver, J.W. Freeman, I. Horvath, W.J. Landis, *Molecular basis for elastic energy storage in mineralized tendon*. Biomacromolecules **2**(3), 750–756 (2001)
50. T.E. Kruger, A.H. Miller, J. Wang, *Collagen scaffolds in bone sialoprotein-mediated bone regeneration*. Sci World J **2013**, **1–6** (2013)
51. F.H. Silver, J.W. Freeman, G.P. Seehra, *Collagen self-assembly and the development of tendon mechanical properties*. J Biomech **36**(10), 1529–1553 (2003)
52. J.P. Orgel et al., *Microfibrillar structure of type I collagen in situ*. Proc Natl Acad Sci **103**(24), 9001–9005 (2006)
53. I. Ahmad, M. Maaza, *Accelerator physics: radiation safety and applications*. BoD–Books on Demand (2018)
54. J.W. Freeman, F.H. Silver, *Analysis of mineral deposition in turkey tendons and self-assembled collagen fibers using mechanical techniques*. Connect Tissue Res **45**(3), 131–141 (2004)
55. Z. Xu, Y. Yang, W. Zhao, Z. Wang, W.J. Landis, Q. Cui, N. Sahai, *Molecular mechanisms for intrafibrillar collagen mineralization in skeletal tissues*. Biomaterials **39**, 59–66 (2015)
56. Z. Xu, W. Zhao, Z. Wang, Y. Yang, N. Sahai, *Structure analysis of collagen fibril at atomic-level resolution and its implications for intra-fibrillar transport in bone biomineralization*. Phys Chem Chem Phys **20**(3), 1513–1523 (2018)
57. F.H. Silver, I. Horvath, D.J. Foran, *Mechanical implications of the domain structure of fiber-forming collagens: comparison of the molecular and fibrillar flexibilities of the α1-chains found in types I–III collagen*. J Theor Biol **216**(2), 243–254 (2002)
58. F.H. Silver, G.P. Seehra, J.W. Freeman, D. DeVore, *Viscoelastic properties of young and old human dermis: a proposed molecular mechanism for elastic energy storage in collagen and elastin*. J Appl Polym Sci **86**(8), 1978–1985 (2002)
59. W. Traub, A. Jodaikin, T. Arad, A. Veis, B. Sabsay, *Dentin phosphophoryn binding to collagen fibrils*. Matrix **12**(3), 197–201 (1992)
60. L. Chen, R. Jacquet, E. Lowder, W.J. Landis, *Refinement of collagen–mineral interaction: a possible role for osteocalcin in apatite crystal nucleation, growth and development*. Bone **71**, 7–16 (2015)
61. W.J. Landis, F.H. Silver, J.W. Freeman, *Collagen as a scaffold for biomimetic mineralization of vertebrate tissues*. J Mater Chem **16**(16), 1495–1503 (2006)
62. W.J. Landis, F.H. Silver, *The structure and function of normally mineralizing avian tendons*. Comp Biochem Physiol A Mol Integr Physiol **133**(4), 1135–1157 (2002)
63. A.K. Nair et al., *Molecular mechanics of mineralized collagen fibrils in bone*. Nat Commun **4**(1), 1–9 (2013)
64. E. Bonucci, *Bone mineralization*. Front Biosci (Landmark Ed) **17**, 100–128 (2012)
65. D. Kim, B. Lee, S. Thomopoulos, Y.S. Jun, *In situ evaluation of calcium phosphate nucleation kinetics and pathways during intra- and extrafibrillar mineralization of collagen matrices*. Cryst Growth Des **16**(9), 5359–5366 (2016)
66. N. Reznikov et al., *Fractal-like hierarchical organization of bone begins at the nanoscale*. Science **360**(6388) (2018)
67. H.P. Schwarcz, E.A. McNally, G.A. Botton, *Dark-field transmission electron microscopy of cortical bone reveals details of extrafibrillar crystals*. J Struct Biol **188**(3), 240–248 (2014)
68. D. Kim et al., *The role of confined collagen geometry in decreasing nucleation energy barriers to intrafibrillar mineralization*. Nat Commun **9**(1), 1–9 (2018)
69. M. Balooch, S. Habelitz, J.H. Kinney, S.J. Marshall, G.W. Marshall, *Mechanical properties of mineralized collagen fibrils as influenced by demineralization*. J Struct Biol **162**(3), 404–410 (2008)
70. P.J. Smeets et al., *Calcium carbonate nucleation driven by ion binding in a biomimetic matrix revealed by in situ electron microscopy*. Nat Mater **14**(4), 394–399 (2015)
71. Y. Wang, T. Azaïs, M. Robin, A. Vallée, C. Catania, P. Legriel, G. Pehau-Arnaudet, F. Babonneau, M.M. Giraud-Guille, N. Nassif, *The predominant role of collagen in the nucleation, growth, structure and orientation of bone apatite*. Nat Mater **11**(8), 724–733 (2012)
72. H. Cölfen, *A crystal-clear view*. Nat Mater **9**(12), 960–961 (2010)
73. F. Nudelman, K. Pieterse, A. George, P.H.H. Bomans, H. Friedrich, L.J. Brylka, P.A.J. Hilbers, G. de With, N.A.J.M. Sommerdijk, *The role of collagen in bone apatite formation in the presence of hydroxyapatite nucleation inhibitors*. Nat Mater **9**(12), 1004–1009 (2010)
74. A.S. Deshpande, E. Beniash, *Bioinspired synthesis of mineralized collagen fibrils*. Crystal Growth and Design **8**(8), 3084–3090 (2008)
75. D.V. Krogstad, D. Wang, S. Lin-Gibson, *Polyaspartic acid concentration controls the rate of calcium phosphate nanorod formation in high concentration systems*. Biomacromolecules **18**(10), 3106–3113 (2017)
76. S. Boonrungsiman, E. Gentleman, R. Carzaniga, N.D. Evans, D.W. McComb, A.E. Porter, M.M. Stevens, *The role of intracellular calcium phosphate in osteoblast-mediated bone apatite formation*. Proc Natl Acad Sci **109**(35), 14170–14175 (2012)
77. M.J. Olszta, X. Cheng, S.S. Jee, R. Kumar, Y.Y. Kim, M.J. Kaufman, E.P. Douglas, L.B. Gower, *Bone structure and formation: a new perspective*. Mater Sci Eng R Rep **58**(3-5), 77–116 (2007)
78. J. Mahamid, A. Sharir, D. Gur, E. Zelzer, L. Addadi, S. Weiner, *Bone mineralization proceeds through intracellular calcium phosphate loaded vesicles: a cryo-electron microscopy study*. J Struct Biol **174**(3), 527–535 (2011)
79. S.S. Jee, L. Culver, Y. Li, E.P. Douglas, L.B. Gower, *Biomimetic mineralization of collagen via an enzyme-aided PILP process*. J Cryst Growth **312**(8), 1249–1256 (2010)
80. L.-n. Niu, S.E. Jee, K. Jiao, L. Tonggu, M. Li, L. Wang, Y.D. Yang, J.H. Bian, L. Breschi, S.S. Jang, J.H. Chen, D.H. Pashley, F.R. Tay, *Collagen intrafibrillar mineralization as a result of the balance between osmotic equilibrium and electroneutrality*. Nat Mater **16**(3), 370–378 (2017)
81. Q. Song et al., *Contribution of biomimetic collagen-ligand interaction to intrafibrillar mineralization*. Sci Adv **5**(3), eaav9075 (2019)
82. J. Mahamid, A. Sharir, L. Addadi, S. Weiner, *Amorphous calcium phosphate is a major component of the forming fin bones of zebrafish: Indications for an amorphous precursor phase*. Proc Natl Acad Sci **105**(35), 12748–12753 (2008)
83. L. Wang, G.H. Nancollas, Z.J. Henneman, E. Klein, S. Weiner, *Nanosized particles in bone and dissolution insensitivity of bone mineral*. Biointerphases **1**(3), 106–111 (2006)
84. M. Kerschnitzki, A. Akiva, A. Ben Shoham, Y. Asscher, W. Wagermaier, P. Fratzl, L. Addadi, S. Weiner, *Bone mineralization pathways during the rapid growth of embryonic chicken long bones*. J Struct Biol **195**(1), 82–92 (2016)

85. A. Akiva, G. Malkinson, A. Masic, M. Kerschnitzki, M. Bennet, P. Fratzl, L. Addadi, S. Weiner, K. Yaniv, *On the pathway of mineral deposition in larval zebrafish caudal fin bone*. Bone **75**, 192–200 (2015)
86. Q. Wang, X.M. Wang, L.L. Tian, Z.J. Cheng, F.Z. Cui, *In situ remineralizaiton of partially demineralized human dentine mediated by a biomimetic non-collagen peptide*. Soft Matter **7**(20), 9673–9680 (2011)
87. F. Nudelman, P.H.H. Bomans, A. George, G. de With, N.A.J.M. Sommerdijk, *The role of the amorphous phase on the biomimetic mineralization of collagen*. Faraday Discuss **159**(1), 357–370 (2012)